Investigating possible mechanisms of Non-Photochemical Laser Induced Nucleation

by

Anshul Sanjeev Garg

in partial fulfillment of the requirements for the degree of

Master of Science
in Mechanical Engineering

at the Delft University of Technology,
to be defended publicly on Thursday August 30, 2018 at 2:00 PM.

Report number :	P&E-2898
Student number:	4557581
Under guidance and supervision of:	Dr. Daniel Irimia
	Dr. H.B. Eral

Thesis committee:	Prof. Antoine van der Heijden,	TU Delft
	Dr. R.M. Hartkamp,	TU Delft
	Dr. H.B. Eral,	TU Delft

An electronic version of this thesis is available at http://repository.tudelft.nl/.

TU Delft Delft University of Technology

Preface

I would like to start by thanking my supervisor Dr. Burak Eral. His invaluable guidance and advice to remain focused towards the objectives of the thesis, helped me to be efficient. The person without whom this thesis wouldn't have been possible is my daily supervisor Dr. Daniel Irimia. The regular discussions about the best way to move forward and about the concepts helped me to think critically at every step.

A special shout out to the NPLIN team for their inputs during the weekly meetings. It provided me with diverse perspectives on how to view a problem and review the work done in the past week, to better plan for the next. It also helped me to keep track of my progress and to be able to finish my thesis on time. Naturally, I'll be defending my thesis during the last NPLIN meeting.

Lastly, I would like to thank my friends and family for keeping me motivated and the wonderful journey that was my masters.

Anshul Sanjeev Garg
Delft, August 2018

Abstract

Crystallization is employed in a wide range of industries but our ability to control it remains far from perfect. New methods are being continuously developed and improved to provide enhanced kinetics and control. Non-photochemical laser induced nucleation (NPLIN) is one of the avenues being looked into extensively since its accidental discovery about two decades ago. Despite providing improved nucleation kinetics and potential polymorph control, the mechanism behind NPLIN is still unknown. Four different theories have been proposed in the literature with varying amounts of agreement between different research groups.

The main aim of this thesis is to try to determine the mechanism behind NPLIN. This report can be divided into two parts, each focusing on a possible mechanism. The first is the optical Kerr effect, which involves investigating the effect of polarization of light on glycine polymorph formed. This is achieved by varying the laser light polarisation and number of pulses for a range of glycine supersaturation. The second part deals with an experimental setup designed to work with microscale volumes. This will give us the capability to isolate the nuclei and observe the events leading up to their formation.

For studying the optical Kerr effect the experiment performed by Sun et al. [1] was repeated. A significant temperature increase inside the solution was obtained because of exposure to a high number of pulses (600) of infrared light. No dependence of laser light polarization on polymorph formation was found. The polymorph formed by laser is different than that obtained by crash cooling. In the second part of the thesis, the attention is shifted towards the role of impurities present in the solution which can also absorb the laser light leading to formation of a cavitation bubble. This possibility was examined with the help of the setup mentioned above. It was noted that the crystals were nucleating at multiple points around the laser focus at a distance which is similar to the size of the cavitation bubble previously reported in literature. These observations made can be attributed towards the presence of a bubble.

Contents

List of Tables

List of Figures

1

Introduction

Crystallization has been used by man since time immemorial, for extracting common salt from sea water or sweet crystals from sugarcane juice. It is a very efficient separation technology with the advantage of delivering a highly pure product in the first go but it is an arduous process to predict. The molecules not only need to coagulate without redissolving into the solution, they also need to be arranged into the fixed lattice. There is still a long way to go for better control of the crystallization process. Nowadays, utilization of external fields (microwave, ultrasound, magnetic and electric field) as tools to improve the nucleation control, crystal growth and structure, has acquired special attention. One such novel method being researched is non-photochemical laser induced nucleation (NPLIN). More about crystallization and NPLIN has been described in the following sections of this chapter.

1.1. Crystallization

Crystallization can be divided into two sub processes. The first is the birth of new crystals known as nucleation. The main driving force is supersaturation which causes a difference in chemical potential of solute in solution and in solid phase. Nucleation can be categorized into primary and secondary nucleation. Primary nucleation is the formation of a stable nucleus from a clear solution due to the interaction between solute molecules. If it happens with the aid of impurities or surfaces then it is called heterogeneous nucleation. In the absence of these, nuclei form by statistical fluctuations of solute entities clustering together which is referred to as homogeneous nucleation. Secondary nucleation entails the presence of crystals and their interaction with the crystallizer environment. It can either take place due to nucleation induced by a crystalline solute, fragmentation of a present crystal, or attrition of a crystal caused by its interaction with the surroundings.

The nucleus grows into a larger crystal by the other sub process, called crystal growth. The parameters affecting this process are the composition and hydrodynamics of the solution. This has been summarized in figure 1.1. In order to describe the rate of nucleation process there are two accepted theories.

- Classical nucleation theory: The classical theory of nucleation employs an addition mechanism by which solute molecules coagulate until a critical radius of the nucleus is reached. This stable nucleus is created by overcoming an energy barrier which is a sum of interfacial free energy and bulk free energy.

- Two step nucleation theory: The two step nucleation theory states that for crystals to be formed two energy barriers need to be overcome. The first barrier involves the formation of a liquid like cluster which is diffusion controlled and the second involves the growth into an ordered crystalline lattice. There has been increasing evidence that NPLIN follows the two step nucleation theory, as it requires the presence of large solute clusters [2]. Such evidence results from the work done on chemicals like glycine as they need to be aged prior to being exposed to laser [1].

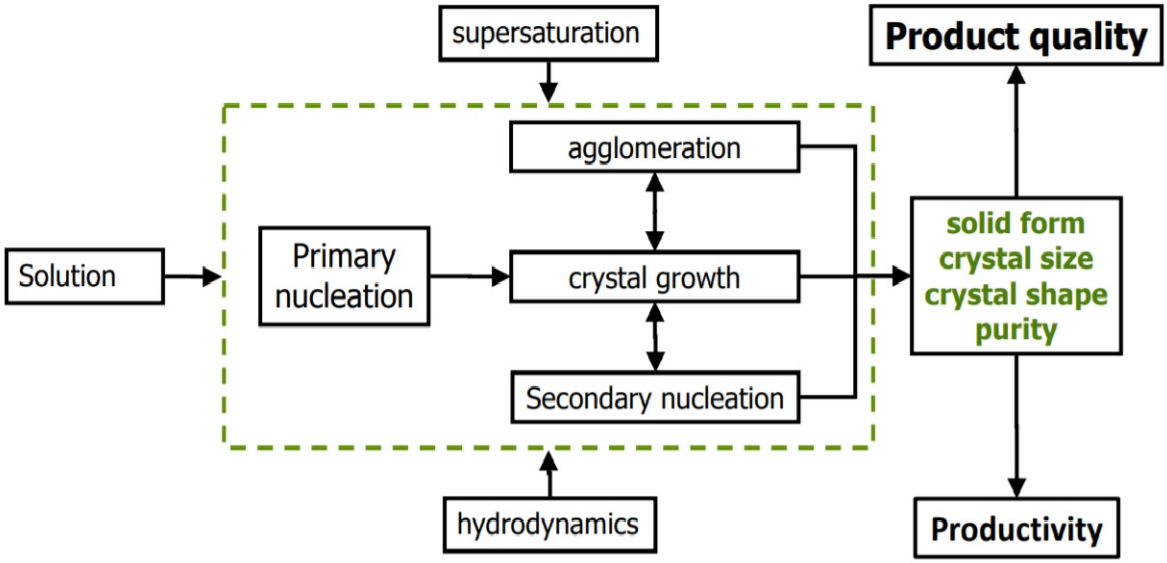

Figure 1.1: Crystallization process

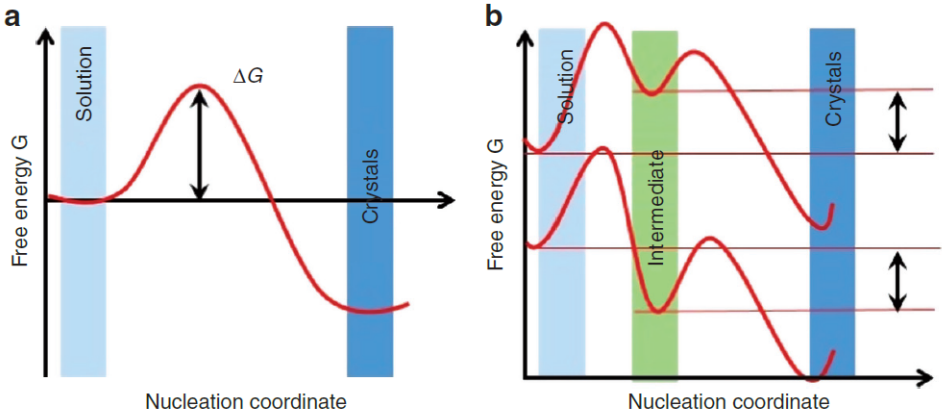

Figure 1.2: Free energy curve

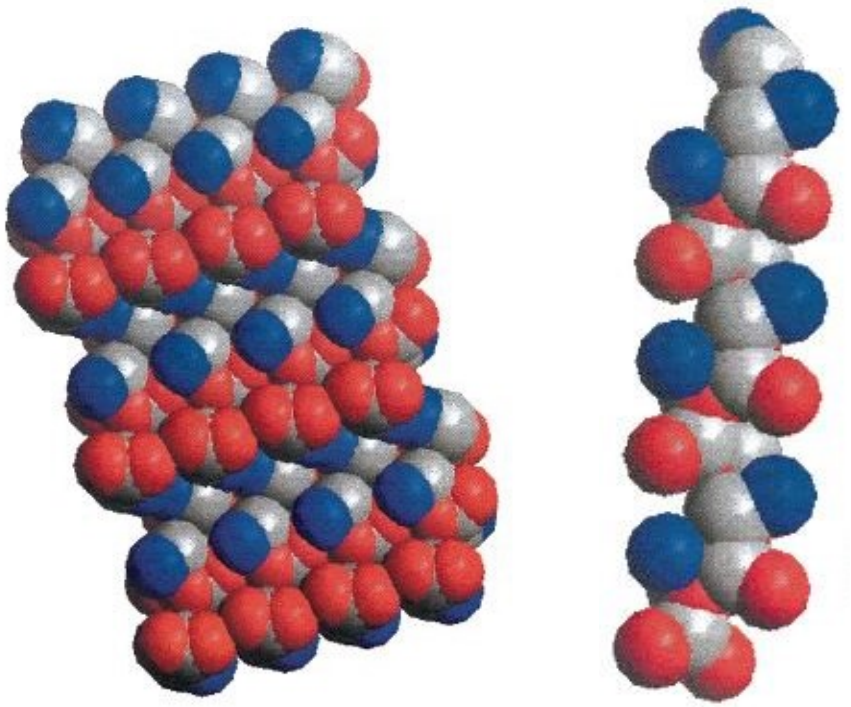

(a) Stacking of alpha polymorph (cyclic dimers)

(b) Stacking of gamma polymorph (helical chains)

Figure 1.3: The packing of molecules for α and γ polymorph. For both parts carbon atoms are in grey, oxygen atoms in red and nitrogen atoms in blue [4]

1.2. Polymorphism

Polymorphism is the tendency of a substance to crystallize into different forms but still remain chemically identical. The polymorphs of a substance can exhibit different physical properties, such as solubility, dissolution rate, melting point and hygroscopicity, which can have a major influence on bioavailability and manufacturing processes of pharmaceuticals and other specialty materials [3]. Garetz et al [3, 4] have proposed a mechanism called optical Kerr effect, which if proven valid can be utilized to crystallize different polymorphs of a substance just by altering the polarization state of light. A detailed description about this mechanism has been given in section 1.3.1. This report will look into the polymorph formation of glycine.

Glycine can exist in five different polymorphic forms α, β, γ, δ and ϵ, of which δ and ϵ can only exist at high pressure conditions. At room temperature β glycine is the least stable polymorph and can only be formed with the help of mixed solvents like ethanol or methanol in water [1]. α and γ polymorphs are both stable at room temperature and can be formed from an aqueous solution. Even though γ glycine is the most stable phase, spontaneous nucleation generally gives the alpha polymorph. This means that spontaneous nucleation of glycine is kinetically controlled rather than thermodynamically [2].

Glycine in aqueous solution always exists as a zwitterion because a proton from the carboxyl group is transferred to the amine group ($^{+}NH_3CH_2COO^{-}$). The basic unit of α polymorph is a cyclic hydrogen bonded dimer. For growth of this polymorph addition of cyclic dimers is required. When the solution becomes acidic or basic, the dipole moment of molecules is reduced thus making cyclic dimer formation less favorable. The structure of γ glycine consists of helical chains of roughly parallel head to tail glycine molecules [4]. The structure of the α and γ polymorph has been given in figure 1.3.

1.3. NPLIN

Non-photochemical laser induced nucleation (NPLIN) is a novel method for nucleation control. In NPLIN experiments, laser light is used to induce nucleation in a supersaturated solution [5]. The

reason as to why this phenomenon is termed non-photochemical is because the solution is transparent to the incoming laser, therefore neither the solute nor the solvent have any absorption bands in the spectral region of the wavelengths used [5]. This phenomenon was discovered accidentally in 1996 by Garetz et al and since then has been observed for glycine, HEWL, urea, histidine, potassium chloride and bromide, supercooled melts of sodium chlorate and glacial acetic acid [6]. Several reports point out that nonphotochemical laser irradiation dramatically reduces the nucleation induction time and controls polymorphism in various fine chemicals relevant for industrial practice [7]. The main governing mechanism remains elusive, although 4 mechanisms have been proposed in the literature. They are described in the following sections:

1.3.1. Optical Kerr effect

In this NPLIN mechanism there is an interaction between the electric field of the light and the molecular components of the solution. Because the electric field at optical frequencies changes its direction on a timescale much faster than the motion of a permanent molecular dipole, it can only align the molecules instead of orienting them. Therefore the electric field induces a dipole moment in the molecules and aligns the most polarizable axis along its direction. Such an alignment leads to minimization of the free energy and allows the molecules to cluster and form a stable nucleus [3, 4, 5, 8, 9]. Optical Kerr effect accounts for the following observations:

- The nucleation probability exhibits linear intensity dependence [10, 11].
- Circularly polarized light favors the alignment of disklike molecules while linear polarization tends to align rodlike molecules. This effect is known as polarization switching and has been observed for L-histidine [3] and glycine [1, 2, 4]. However it should be noted that polarization switching has not been reproduced by any other research group so far [12].
- In the case of urea, a lower power threshold and higher nucleation efficiency was obtained for linearly polarized light as compared to circularly polarized light due to stronger alignment by the former.

The magnitude of field-induced dipole interaction energy is $10^{(-4)} * kT$, where k is the Boltzman's constant and T is the room temperature. This value is negligible as it only represents around 1° of alignment [4]. The optical kerr effect cannot account for increased stability of α or γ glycine as the interaction energies are far too small. Hence it influences the kinetics rather than the thermodynamics. As the induction time has been decreased from days to seconds, a reduction in activation barrier of 30 kT is required according to classical kinetics. Even for a cluster containing hundreds of molecules, the barrier is only reduced to 0.03 kT which is 1000 times too little [4]. Therefore the strength of the electric fields does not appear to be high enough to considerably reduce the activation barrier. There are also some other observations that this mechanism cannot explain:

- The organisation of KCl crystals as well as acetic acid do not follow the optical Kerr effect [10, 13].
- Some chemicals like KCl show no polarization dependence and no preferable polarization axis [13] and even with a mismatch between polarizable axis and polarization of light, NPLIN can still occur [14].
- Optical Kerr effect also cannot explain the laser induced nucleation of CO_2 bubbles in supersaturated carbonated water [15].

1.3.2. Isotropic electronic polarization

Another mechanism suggested in literature is isotropic electronic polarization. This in no way contradicts the optical Kerr effect but is used to explain the NPLIN effect for molecules like KCl which assemble in a simple cubic structure [8]. This mechanism is based on a two-step model as it requires the presence of solute clusters in solution. When a dielectric particle is immersed in a medium with lower dielectric constant, its free energy is reduced in the presence of a static electric field [8, 13, 14]. Thus a supersaturated solution will now have a few of the solute clusters lying in the supercritical region of the modified free energy curve [8, 13]. This theory is mainly supported by the time scales for movement of the large ions which is approximately 100 ps, and falls well within the 5 ns duration of the laser pulse

[8]. The drawback of this mechanism is that it predicts a zero threshold for the power density of the laser which is in direct contradiction to the experimental observations [8, 13]. As a theoretical model developed by Alexander et al [13] accounts only for the clusters that become supercritical, in order to calculate the total clusters in the solution an empirical factor k is used. Only when the threshold is added and the factor k is taken into account can the experimental results be reproduced by the model. Even so, the model agrees to some extent with KCl experiments but not with KBr results. The reason for the drawbacks is that the interfacial tension does not take into account the internal dynamics and structure of the cluster.

1.3.3. Shockwave crystallization

Nasrin et al [16] were able to induce nucleation by focussing the laser 5 cm into an aqueous supersaturated solution. The nucleation wasn't only limited to the focal volume because of the pressure and temperature variations caused throughout the solution by the compression sound waves. They also conducted experiments in which a laser focused onto a thin metal boat floating on top of a solution resulted in formation of crystals. Sodium bromate, sodium chloride and tartaric acid were nucleated by this method. The drawback with their method was the utilization of very high powers, 10^4 higher than the powers used by Garetz in the original article.
To investigate the role of pressure waves for NPLIN, Kacker et al [7] compared nucleation in masked and unmasked vials. Although a much higher-pressure signal was measured in masked vials compared to unmasked vials, no nucleation was observed. As unmasked vials showed nucleation, it proved that pressure waves do not play a crucial role in their experiments.

1.3.4. Nano-impurities

It is nearly impossible to make absolutely pure solutions, even in controlled laboratory conditions. The impurities can come from the constituents of the solution, or can be inadvertently introduced during the preparation process. Many experiments have been conducted to study the influence of these impurities on NPLIN. It has been observed for different chemicals that filtration of samples has a significant effect on the nucleation probability as well as the number of nuclei formed. Alexander et al found out that an increase in purity of aqueous KCl solution leads to a decrease in the lability. It was also observed that solutions which were not passed through 0.2 µm filters were significantly more prone to nucleate [13]. In another laser based experiment conducted on ammonium chloride the same group obtained a stark difference in the probability between filtered (p=0.65) and unfiltered samples (p=1). Filtered samples on average produced 1.4 ± 0.4 nuclei, in contrast with 7.8 ± 1.3 nuclei obtained by the unfiltered ones. It was found that the nucleation probability and average number of nuclei produced (1.0 ± 0.0) in control samples (pure aqueous solution) were very similar to those obtained by filtered samples in earlier experiments. Further on, the filtered solutions were doped with Fe_3O_4 nanoparticles. This addition removed any effect that filtration might have had. All of the doped samples nucleated and the number of nuclei produced were quite similar to the unfiltered samples [11]. Javid et al also conducted a filtration experiment with aqueous glycine. At all supersaturations (1.4,1.5,1.6) nanofiltration of glycine gave huge difference in nucleation probability [17]. Ward et al also observed that nucleation is mostly caused by a species which can be removed by filtration, and the main source of impurities was the solute [12]. Kacker et al showed that samples passed through a 0.45 µm syringe filter resulted in significantly reduced nucleation probabilities for KCl [7].
With the insurmountable experimental proof for the role of impurities, the interaction proposed mostly between the impurities and the laser is via heating. When the solution is exposed to the laser light, the impurities absorb some of its energy, heating the surrounding molecules. The solvent evaporates and starts to form a vapour bubble that expands explosively, leading to a shock wave emission.The volume of the vapor bubble then expands with a velocity smaller than that of the shock wave. The expansion then slows down and after reaching a maximum, the bubble begins to collapse. Velocity reduces due to a rapid pressure drop within the cavity. The collapse phase is relatively gradual, as well as the rate of the energy released is low [18, 19, 20]. The collapse of the cavity is followed by formation of many small gas bubbles. The explanation for their formation varies. The small bubbles are probably caused by the boiling of solvent, which is initiated by local heating due to adiabatic compression in the collapse process. Additionally, jet flow generated by an asymmetry collapse of the cavity creates an asymmetrical convection around the laser focal point. This convection would split the produced gas bubble into a few [18]. The small gas bubbles that are formed initially and contain non-condensable

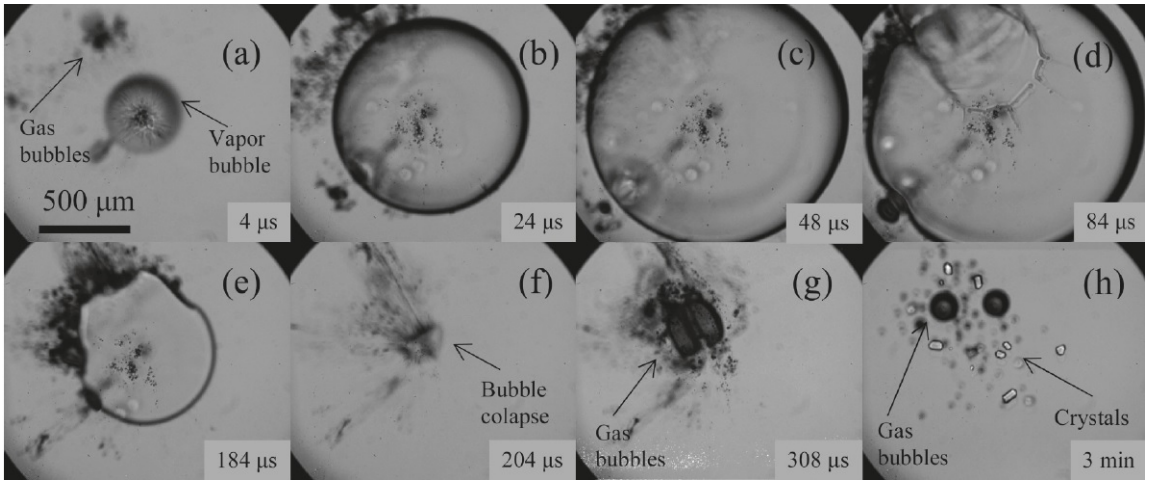

Figure 1.4: Cavitation observed by [19]

air, remain after the collapse [19]. As the cavity walls decelerate, a rarefaction wave propagates away from the center of the bubble and results in a tension field which causes many small bubbles to form in the focal region. These bubbles grow slightly and persist for about 100-200 µs, depending on their size, then collapse and disappear [20].
A few different ways have been proposed for the nucleation of crystals via cavitation bubble.

- The expanding bubble accumulates the solute on its surface leading to increase in local supersaturation. This may be due to thermal convection and Marangoni convection [21], reduced spatial dimensionality of the interface which enhances the potential for aggregation [12], adsorption of molecules at the surface of bubbles featuring lifetime of a few seconds [18], greater diameter of cavitation bubble than diffusion length which can cause the local molecular condensation [22].

- The expanding bubble surface may function as a nucleation site because the free energy barrier for heterogeneous nucleation is lower as compared to homogeneous nucleation [9].

- Pressure fluctuations are created during the shockwave emissions in the order of GPa, also during explosive expansion and collapse of the bubble in the order of MPa. These fluctuations could be the required disturbances in the solution to induce nucleation [18, 22].

There has been a lot of support for cavitation bubble being an intermediate for nucleation. Nakamura et al [18] observed bubbles in the vicinity of the focal point 0,67 ms after firing the laser, followed by crystalline objects after 300 ms. Experiments performed by Soare et al [19] show that a vapor bubble is observed at the focal point of the laser after 4 μs. 50 µs later, a thin ring shaped optical disturbance is observed surrounding the focal spot. After 1 sec a ring of small crystals is observed at the same place as the disturbance. These developments have been shown figure 1.4.

Not only has it been shown that bubble formation may cause crystallization but is a precursor for it. The threshold for cavitation bubble generation is in good agreement with that of crystallization [18, 23]. Yoshikawa et al [22] observed higher threshold energy for crystallization than for cavitation bubble generation. The difference in threshold contributes to the induction of protein nucleation. No crystallisation was obtained below a certain threshold, even for very high supersaturation. This threshold corresponds to that required for cavitation bubble.
To further substantiate the role of bubbles for nucleation of crystals, Knott et al [15] cosupersaturated an aqueous glycine solution with argon. The aqueous solution of glycine and argon was shaken gently which resulted in formation of a large number of argon bubbles. The formation of bubbles was followed by visible glycine crystals throughout the solution. Nucleation and crystal growth continued for several minutes thereafter. To make sure that argon bubbles formation is a factor leading to nucleation of glycine, two control experiments were performed. One was without argon and the other only saturated with argon. In the control experiments a few bubbles were observed but this was due to entrainment of air. The experiment with saturated argon solution was performed once and no crystals were obtained.

The one without argon was performed twice, one instance giving no crystals and the other only a few. There are still some aspects of NPLIN that cannot be explained by the impurity-heating mechanism-

- The occurrence of polarisation switching effect in compounds like glycine [2, 12, 14].
- NPLIN does not occur for all the compounds. It was observed by Ward et al [14] for aqueous solution of potassium acetate but not for sodium acetate.

1.4. Thesis Objectives

The main objective of this work is to bring additional insight about the mechanism behind NPLIN. For this purpose the following tasks were carried out:

- Measure the energy absorbed and the resulting temperature rise to quantify the effect of the number of pulses during laser exposure of a glass vial containing aqueous supersaturated glycine solution.
- Observe the effect of supersaturation on polymorph formation of glycine.
- Quantify the effect of laser on nucleation of glycine and subsequently confirm the presence or absence of a polarization switching window.
- Design an experimental setup to observe the formation of a cavitation bubble leading to formation of crystals in a supersaturated aqueous KCl solution.

2

Influence of laser irradiation

To get a better idea about the NPLIN mechanism, the laser light properties and the solution parameters need to be carefully studied. This chapter deals with the effect of supersaturation, light polarization and the number of laser pulses on an aqueous glycine solution.

2.1. Materials and Methodology

2.1.1. Materials

Glycine (Sigma-Aldrich, puriss, buffer substance, 99.7-101%) without any further purification is dissolved in distilled water (Elga Purelab Ultra, 3.7 MΩ.cm) to prepare a supersaturated solution. Four different supersaturations of 1.4, 1.5, 1.6 and 1.7 are prepared for the experiments mentioned in this chapter.

2.1.2. Sample preparation

Preparation of glycine requires careful handling at each step as every small detail affects the time required and the final number of usable vials for laser exposure. To prepare the stock solutions, the quantities of glycine mixed with 1 kg of water are 343, 367.5, 392 and 416.5 grams corresponding to supersaturations of 1.4, 1.5, 1.6 and 1.7 respectively at 24 °C. The optimum way of dissolving glycine is to keep the mixture in the oven at 65 °C for approximately 2 days with occasional stirring. A slightly higher temperature of 70 °C is required for supersaturation of 1.7.
The stock solutions are then transferred to small cylindrical borosilicate glass vials of volume 8 ml and diameter 1.3 cm. After a few trials, the following procedure is found to be efficient. Small amount of stock solution is taken into a clean beaker maintained at 65 °C and continuously stirred. A new syringe and needle is used every time to transfer the solution into a vial. As soon as 10 of them are fully filled they are transferred into the oven also maintained at 65 °C. This is repeated for the entire stock solution. The prepared vials are then kept in the oven to assure that the glycine remains dissolved.
After a few days, the vials are transferred into water baths and cooled down gradually over the course of a day from 65 to 24 °C at a rate of 5 °C/3 hr. The vials are then kept in the water bath for almost a week to check for spontaneous nucleation. This is only done for a few initial batches to make sure the laser induced nucleation is not affected by spontaneous nucleation. Using the methodology described above very low number of vials crystallized spontaneously, generally only 1 or 2 out of 150. Before starting the experiment, a run without laser is done to confirm that accidental handling/shaking of vials (during removal and placement into water baths) does not affect the nucleation.

2.1.3. Experimental layout

A Q-Switched Nd:YAG laser (Continuum Powerlite DLS 8000 model) is used to perform the experiments. It produces a train of light pulses at a fundamental wavelength of 1064 nm and a repetition rate of 10 Hz. By utilizing second harmonic generation and third harmonic generation processes in potassium dihydrogen phosphate non-linear crystals, 532 nm and 355 nm respectively can be produced. For the experiments described in this section only the fundamental wavelength of 1064 nm at maximum power

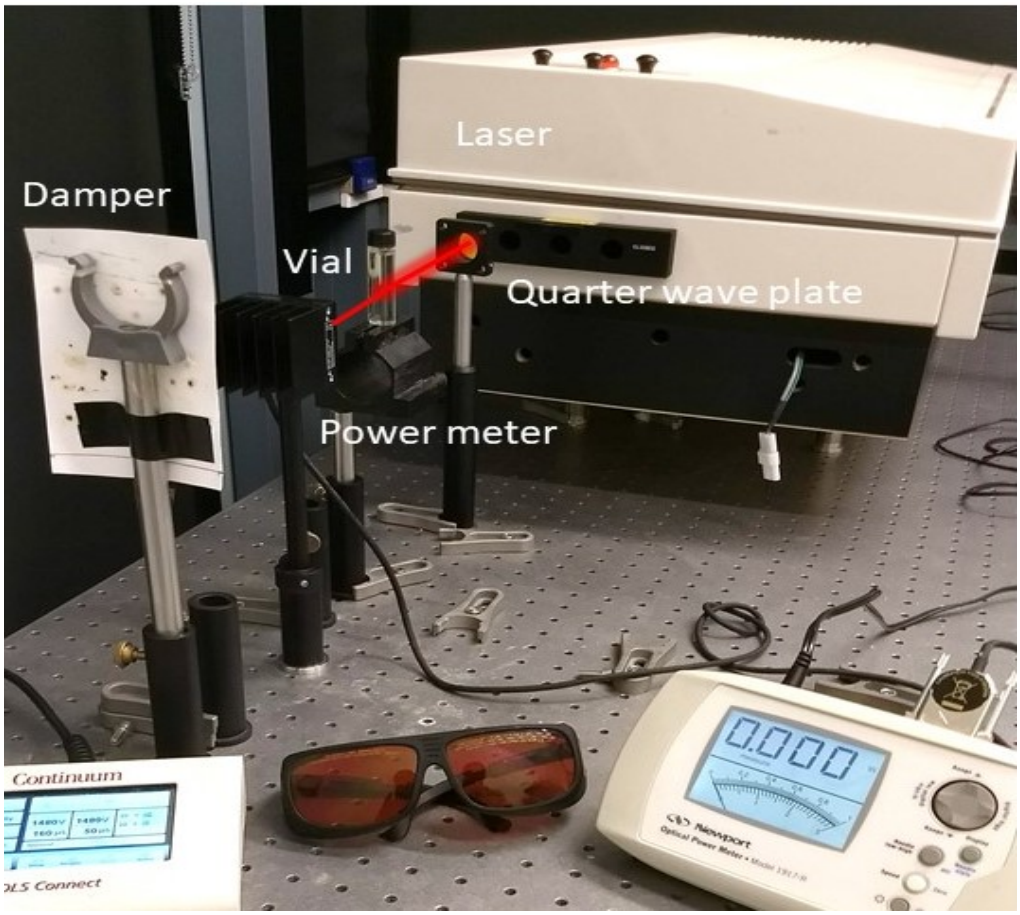

Figure 2.1: Experimental setup for exposure to 1064 nm and circularly polarized light

of 10 W and a full beam diameter (9 mm) is employed. Using the full beam diameter helps to simplify the setup as a telescope is no longer required. 1064 nm is employed to compare the effects of polarization of light on the glycine polymorphism with results presented in the literature [1, 17, 24, 25]. The likelihood of damaging the vials at this wavelength is also reduced as the vial which behaves as a cylindrical lens focuses the laser light at a much farther distance as compared to the shorter wavelengths. The power of the light pulses is measured by 2 power meters, 818P High Power Newport detector and Gentec Electro Optique Maestro. The time duration(~7 ns) of the laser pulses is accurately measured using a Thorlabs Det10A high speed photodetector and visualised on an Agilent oscilloscope.
The aged vials are then exposed to laser light of different parameters using the setup given in figure 2.1. A quarter wave plate is added only when the polarization of light needs to be changed from linear to circular. A proper alignment of the quarter wave plate ensures a constant power of the beam behind a Glan-Taylor Calcite Polarizer(GL-10) regardless of the orientation of its axis.

2.1.4. Postprocessing

Soon after laser exposure, the vials are transferred into the water bath at 24°C to maintain the same supersaturation. The vials which nucleated are noted at different time intervals 7, 24 and 48 hours. Powder X-ray diffraction is used to detect the type of polymorph that formed. The procedure depicted by Boldyreva et al [26] is followed as it ensures stability of the polymorphs throughout the analysis. Crystals are first washed with deionized water and then dried using compressed air before being ground into powder using a mortar and pestle. The PXRD results are compared with the database spectra for the identification of alpha and gamma glycine.

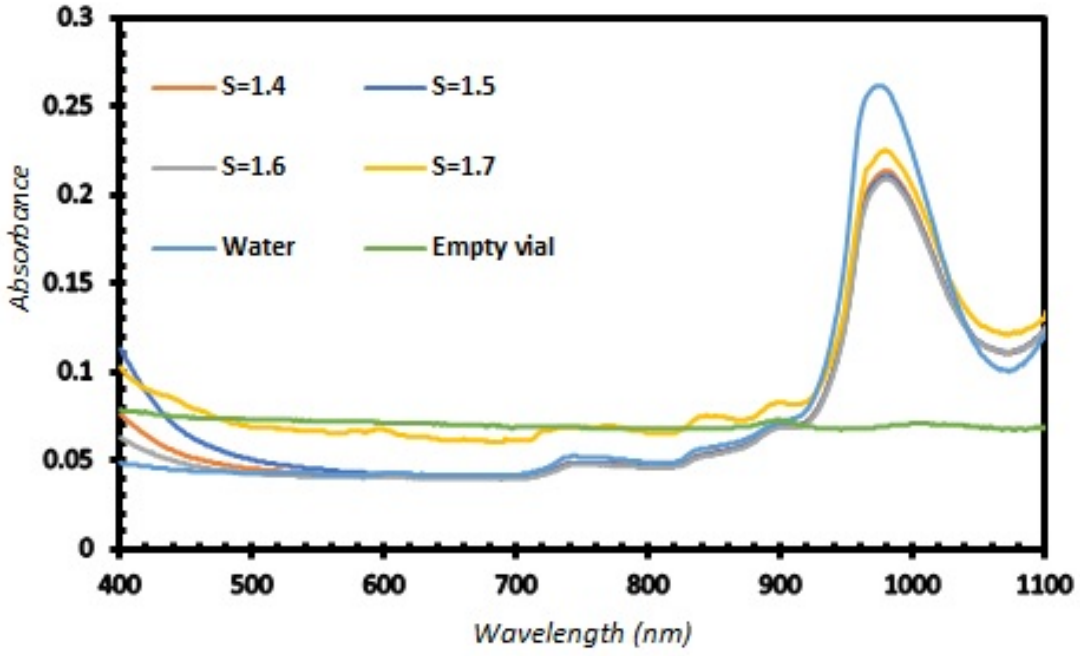

Figure 2.2: The VIS-IR spectrum for different supersaturations of glycine, water and empty cuvette.

2.2. Absorption of laser light

Although the solution is transparent to the incident laser light, there still is a slight absorbance by glycine and water in the near infrared region. Furthermore, there are also reflections at the air-glass interfaces. In this section the absorbance and reflections are quantified at both 532 nm and 1064 nm as well as for both 1 and 600 pulses. The resultant effect on supersaturation and mixing is also looked into.

2.2.1. UV-VIS spectrum of glycine

The absorbance of aqueous glycine solutions at different supersaturations between 1.4 and 1.7 is measured with a UV-VIS spectrophotometer (Hach DR6000). The absorbance is measured over the spectral range of 400-1100 nm at a rate of 900 nm/min. The spectrum obtained for various supersaturations of glycine is displayed in the figure 2.2, which shows that the absorbance doesn't vary significantly with supersaturation.

The energy absorbed by the glycine solution is calculated by the definition of absorbance, which is given as follows:

$$A = log_{10}\frac{I_O}{I_T} \tag{2.1}$$

Where,
A=Absorbance as obtained from the UV-VIS spectrophotometer.
I_O= Incident intensity on vial in Joule.
I_T= Transmitted Intensity in Joule.
On rearranging the above equation and taking incident intensity as the sum of absorbed and transmitted intensities, we get the value of absorbed intensity (I_A) by the following formula

$$I_A = I_O * (1 - 10^{-A}) \tag{2.2}$$

In our experiments powers of 10 W at 1064 nm and 3.2 W at 532 nm are used which correspond to energies of 1 J and 0.32 J per pulse respectively. The density of the glycine solution is calculated experimentally by measuring the mass of the solution for a known volume. This is repeated a few times to reduce the measurement error. Based on the specific heat capacity value obtained from Lark

Table 2.1: Change in supersaturation and temperature of glycine solution due to energy absorbed from laser

Supersaturation	Wavelength (nm)	Absorbance	Absorbed Energy (J) (1 pulse)	Specific heat capacity ($J/(g*K)$)	Density (g/cm^3)	Δ T ($^\circ C$) (600 pulses)	Supersaturation after exposure to 600 pulses
1.4	532	0.043	0.0301	3.23	1.096	0.594	1.385
	1064	0.112	0.227			4.479	1.272
1.5	532	0.046	0.0321	3.18	1.108	0.636	1.483
	1064	0.112	0.227			4.501	1.363
1.6	532	0.042	0.0295	3.13	1.12	0.587	1.583
	1064	0.112	0.227			4.524	1.453
1.7	532	0.067	0.0457	3.07	1.132	0.918	1.669
	1064	0.123	0.246			4.951	1.530

et al [27], the temperature increase (ΔT) is determined from the following formula.

$$\Delta T = \frac{I_A}{c_p * m} \tag{2.3}$$

Where,
c_p= Specific heat of aqueous glycine in $\frac{J}{g*K}$.
m= mass of solution per vial in g.
The increase in the solution temperature due to the laser exposure results in a change of supersaturation which is calculated by using the solubility curve obtained from 'An Encyclopedia of Chemicals, Drugs, and Biologicals' [28]. The change in temperature and supersaturation as well as the density, specific heat and absorbance values are shown in table 2.1.

It can be observed from the table that there is a consistent change in supersaturation of about 0.15 caused by exposure of solution to 600 pulses at 1064 nm. At 532 nm such change is negligible.

2.2.2. Temperature measurements

To validate the calculations mentioned in the previous section, the temperature of glycine solutions of S=1.5 and 1.6 and distilled water is measured experimentally by a thermocouple before and after exposure to 1064 and 532 nm. The results obtained are given in tables 2.2 and 2.3. It is worth noting that the insertion of thermocouple into the solution during exposure can lead to formation of glycine crystals which can absorb additional energy from the laser. Therefore it's advisable to measure temperature of the solution at the end of the exposure cycle.

It can be seen from table 2.2 that there is significant absorption by water as well as glycine solution at 1064 nm. The absorption in the glycine solutions is nearly similar at both supersaturations of 1.5 and 1.6. An average temperature increase of 4.4°C is obtained for an aqueous glycine solution as compared to 3.2°C for pure water. The absorption is stronger at 1064 nm than 532 nm where only a negligible temperature rise is observed. The temperature measurements are in good agreement with the calculations based on the absorbance data from UV-VIS spectrophotometer.
The absorption of 1064 nm light photons during the 1 minute exposure results in an upward temperature gradient of about 0.5 °C/cm between the top and bottom of the vial. As the laser is fired just at the bottom part of the vial, the presence of this gradient involves convection and implicitly mixing in the solution. No temperature gradient is observed at 532 nm as there is no absorption at this wavelength.

2.2.3. Loss in laser power

In addition to the absorption by solution, some of the laser energy is lost by reflection off the glass walls of the vial due to the change in refractive index at the air-glass and glass-air interface. This reduction in laser energy was measured experimentally for both 1064 nm and 532 nm with the Newport power meter. The readings of the power meter before and after the vial are shown in figure 2.3.

For an empty vial the laser light first transitions from air to glass followed by glass to air which is repeated as the laser light exits. In total, there are four glass-air interfaces and the amount of reflections is equal for each of them. Hence for a loss of 1 W in an empty vial (from figure 2.3), every surface

Table 2.2: Increase in temperature due to exposure to 600 pulses at 1064 nm and 10 W. '*' denote the points where temperature measurements are only made in the end

Vial	S=1.6		S=1.5		Demi-water	
	Initial Temperature °C	Final Temperature °C	Initial Temperature °C	Final Temperature °C	Initial Temperature °C	Final Temperature °C
1	23.9	28	24.3	28.5	24.1	27.5
2	24.2	28.7	24.5	28.9	*	27.3
3	*	28.1	24	28.4	*	27.7
4	*	28.3	24.1	29.3	24	27.4
5	24.2	29.7	*	28.1	*	27.3
6	24.6	28.3	*	28.3	*	27.3
7	-	-	*	28.7	*	26.9
8	-	-	*	28.1	*	26.9
9	-	-	*	28.2	24.1	27
10	-	-	*	28.4	24	27.2
11	-	-	-	-	24	27.1
12	-	-	-	-	24	27.1

Table 2.3: Increase in exposure due to 600 pulses at 532 nm and 3.2 W. '*' denote the points where temperature measurements are only made in the end

Vial	S=1.6		Demi-water	
	Initial Temperature °C	Final Temperature °C	Initial Temperature °C	Final Temperature °C
1	*	24.5	*	24.5
2	24.3	25.0	*	24.5
3	*	24.7	24.1	24.7
4	24.3	24.9	24.1	24.6
5	*	24.7	*	24.6
6	*	24.4	24.2	24.7
7	24.3	25.0	*	24.5
8	*	24.7	24.1	24.5

contributes by 0.25 W. When a solution is added to the vial the number of interfaces are reduced from 4 to 2 due to the similar refractive index of glass and solution. This becomes obvious from the power measurements at 532nm, showed in figure 2.3, where an increase in exit power is obtained when the glass vial is filled. The same occurs also at 1064nm but the power enhancement is not observed due to solution's absorption of laser photons at this wavelength. For a water solution exposed to infrared light, the power absorbed is 1.7 W while the loss by reflections is reduced to 0.5 W. The total energy absorbed is 0.17 J per pulse and 102 J after exposure to 600 pulses. The heat capacity of water is 4.186 J/g*K leading to a temperature rise of 3 °C in a volume of 8 ml. This is in good agreement with the temperature measurement results.
Computed in a similar way the power absorbed by the glycine solution is 2 W. This corresponds to energy absorbed from a single pulse to be 0.2 J which is quite similar to the values reported in table 2.1 calculated from the absorbance values obtained by UV-VIS spectroscopy.

2.3. Results

With the given experimental layout the laser parameters whose effects have been studied are the polarization of light (linear v/s circular) and the number of pulses (1 v/s 600). These parameters were tested at different supersaturations(1.4, 1.5, 1.6, 1.7), so a control case of crash cooling at each supersaturation was done. All the graphs shown in this section contain error bars with 95% confidence

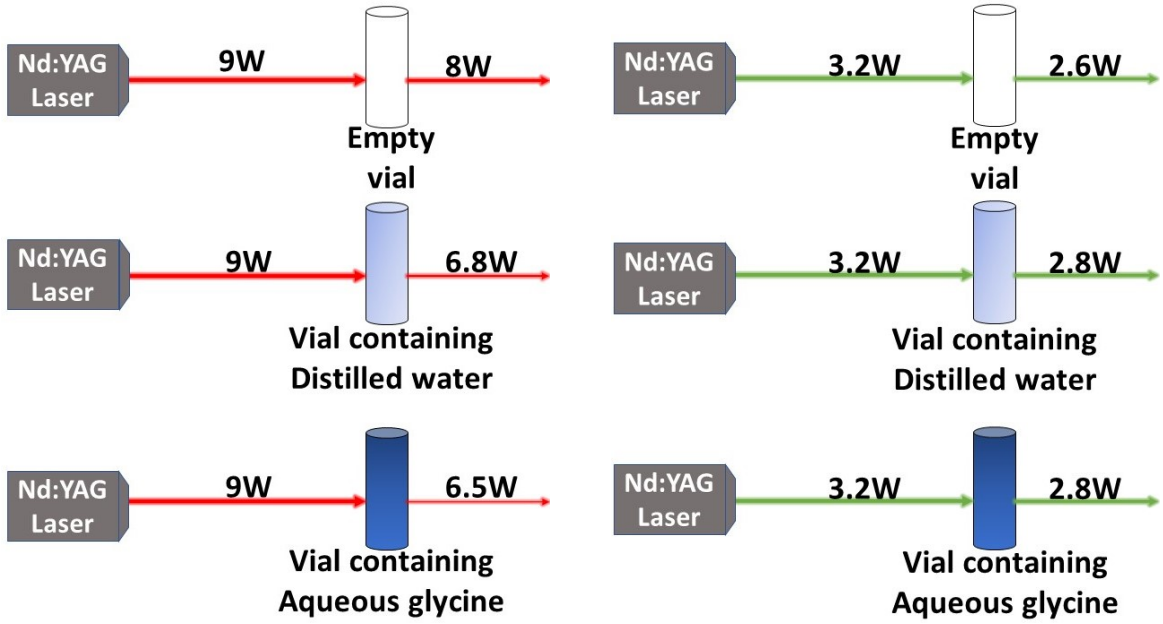

(a) 1064 nm (b) 532 nm

Figure 2.3: Reduction in laser power when it goes through a vial

limit, and all the values obtained have been given in Appendix A.

2.3.1. Effect of supersaturation

This section provides us a basis for quantification of the effect of laser on nucleation both in terms of induction time and polymorph formation. This is achieved by crash cooling the vials from 65 °C to 24 °C by directly transferring them from the oven into the water bath. The crystallization was monitored for 5 days and the cumulative probability distribution has been shown in figure 2.4(a).
It can be seen from this figure that glycine crystallizes rather slowly and has a long induction time. The percentage of gamma polymorph crystallized by this method has been shown in figure 2.6(a). The formation of gamma polymorph increases with supersaturation.

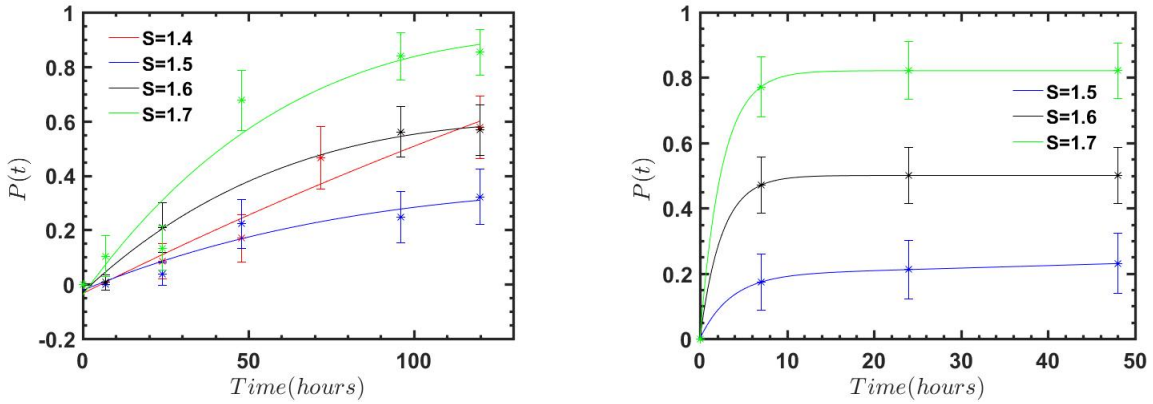

(a) Cumulative probability distribution for nucleation due to crash cooling at different supersaturation

(b) Cumulative probability distribution for nucleation due to laser exposure at different supersaturation. Samples exposed at 1064 nm, 10W, linear polarised light and 1 pulse

Figure 2.4: Increase in nucleation caused due to exposure to laser as compared to crash cooling

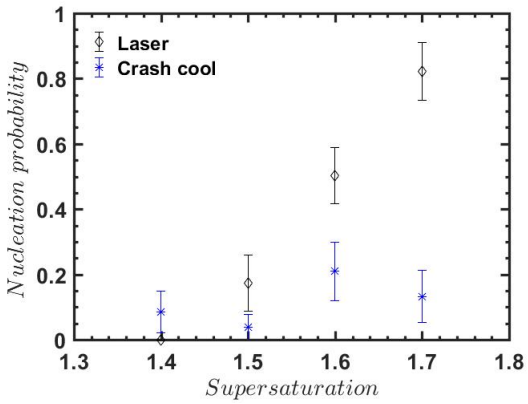

(a) Probability of nucleation comparison between laser and crash cooling at 24 hours.

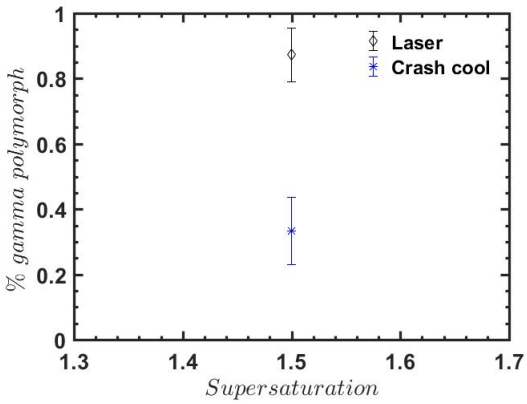

(b) Percentage gamma polymorph obtained by crash cooling versus laser after 24 hours. Samples exposed to laser light at 1064 nm, 10W, linearly polarized and 1 pulse.

Figure 2.5: Glycine nucleation caused by crash cooling versus laser exposure

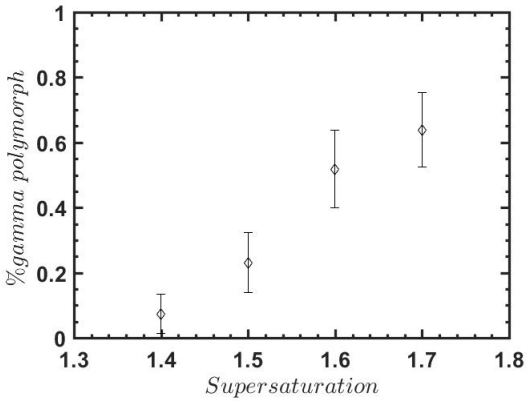

(a) Effect of supersaturation on % of gamma glycine formed. The data represents the cumulative result for crash cooling after 5 days (120 hours).

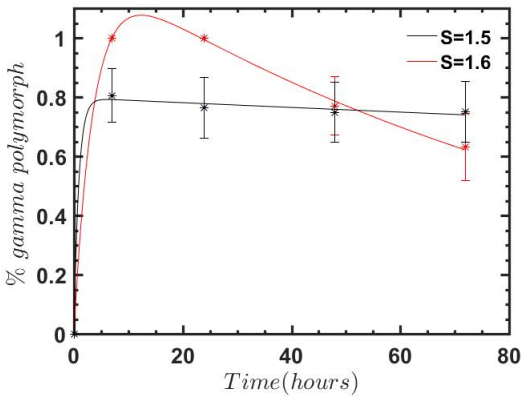

(b) Cumulative probability distribution of formation of glycine polymorph by exposure to laser at single pulse 1064 nm, 10W and circularly polarised light

Figure 2.6: Gamma polymorph formation by crash cooling versus the laser

2.3.2. Effect of laser exposure

The graphs in figure 2.4 show that the laser can significantly reduce the induction time of crystallization. A similar result has also been obtained by Kacker et al [7] in their KCl studies. As compared to the trends obtained in figure 2.4(a), it can be seen that for the case of NPLIN, the majority of nucleation occurs within 7 hours irrespective of supersaturation. To observe in more detail the difference in amount of nucleation a direct comparison between crash cooling and NPLIN within a 24 hour time window is displayed in figure 2.5 (a). The comparison has been done at 24 hours and not 7, because no nucleation is observed for crash cooling in the first 7 hours.

It can be seen from figure 2.6 that the use of laser increases significantly the tendency of formation of gamma polymorph at supersaturations of 1.5 and 1.6. To reinforce this fact, a comparison at 24 hours for the percentage of gamma polymorph formed via laser versus crash cooling has been shown for a supersaturation of 1.5 in figure 2.5 (b). The appearance of alpha polymorph also increases with time due to spontaneous nucleation. As observed previously in figure 2.4(b) the laser effect is generally limited to the initial 7 hours and beyond that time spontaneous nucleation takes over. This claim is also supported by Liu et al [24] and Javid et al [17] who argue that spontaneous nucleation regime takes over the NPLIN regime with time.

The glycine solution of supersaturation 1.4 was not exposed to single pulse at 1064 nm and 10 W

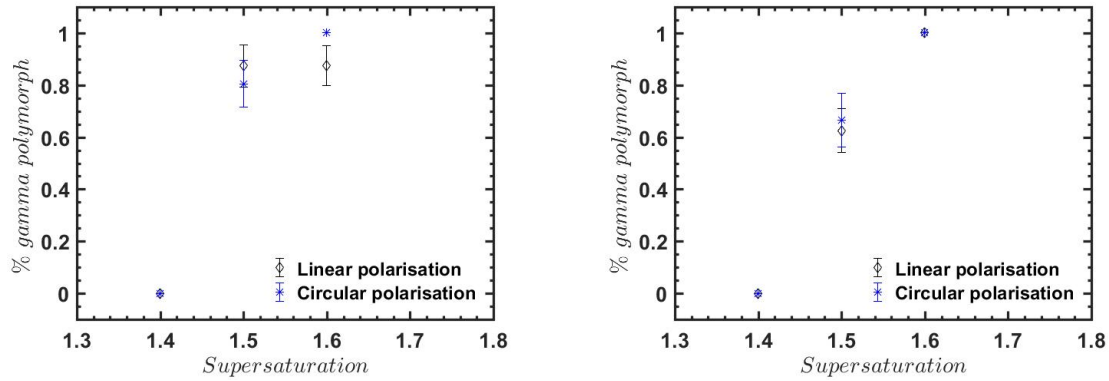

(a) 1 pulse of 1064 nm is utilized

(b) 600 pulses of 1064 nm is utilized

Figure 2.7: Comparison of % gamma polymorph formation between use of linear and circularly polarized light after 7 hours.

due to the fact that a previous exposure to higher number of pulses resulted in very low nucleation probability. Only 3 out of 156 vials crystallized after irradiation to 600 pulses at 1064nm and none of the 35 samples crystallized after exposure to single pulse at 532 nm. To get more nucleation at this supersaturation, the laser power density is increased by shrinking the beam diameter from 9 mm to 4.5 mm via a lens telescope. After increasing the intensity by 20%, 142 vials (divided equally among LP and CP) were exposed but no nucleation was observed within 24 hours. During such exposure 5 vials were damaged due to ablation at high peak energies. For the next two trials, only 1 out of 37 and 1 out of 50 samples crystallized. In overall, the samples (5 vials) at S=1.4 that crystallized within 7 hours after three rounds of experiments turned out to be alpha glycine.

2.3.3. Effect of polarization and number of pulses

As depicted in the previous section, the polymorphism is dependent on the supersaturation. This section will provide a better insight into the effect of laser light on the polymorph formed. Figure 2.7 shows the relation between the laser polarization and the formation of gamma polymorph after exposure to near infrared light.

It appears that there is no difference between the percentage of gamma polymorph obtained with either linearly or circularly polarised light at supersaturations ranging from 1.4-1.6. The polarization switching window reported by Sun et al lies between the supersaturations of 1.45 and 1.55, but no such window has been observed in our experiments. By comparing figures 2.7(a) and (b) one can be observed that results are independent of the number of pulses.

Figure 2.8 shows that the change of polarization state of light (linear to circular) doesn't affect the nucleation probability as well. Furthermore, it can be seen that the variation in number of light pulses does not affect the nucleation probability either and the use of a single pulse is sufficient to trigger NPLIN. When the vials are being exposed to 600 pulses there are two competing phenomena affecting the nucleation rate. The reduction in supersaturation due to absorption causes the rate to decrease whereas the mixing induced by the temperature gradient causes the rate to increase. The fact that no difference in amount of nucleation is observed between 1 and 600 pulses hints towards the fact that the overall change in nucleation rate is insignificant.

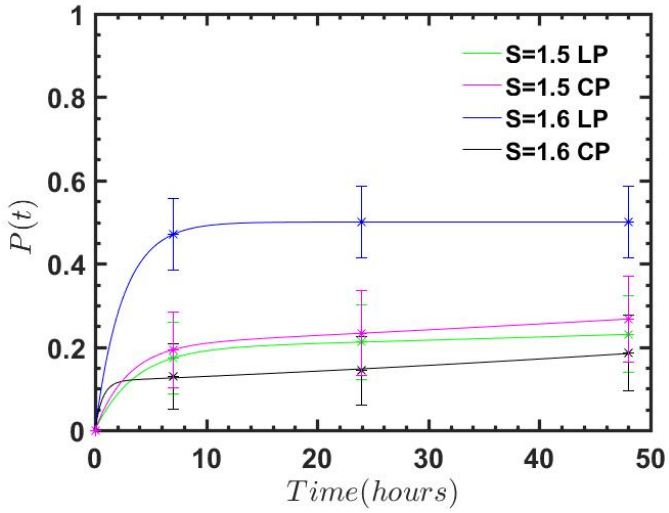

(a) 1 pulse of 1064 nm is utilised

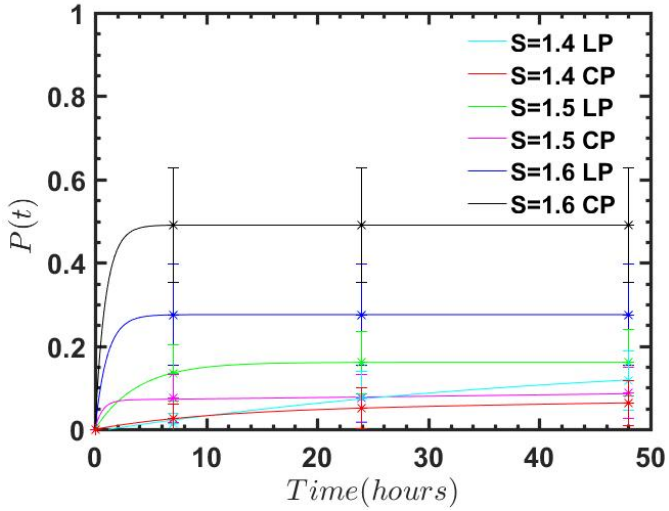

(b) 600 pulses of 1064 nm is utilised

Figure 2.8: Comparison of cumulative probability distribution for nucleation between use of linear and circularly polarized light.

3

Experiment design for cavitation

In this chapter an experimental setup has been designed to study with greater detail the effect of presence of impurities in the solution and their role via the cavitation mechanism explained in the section 1.3.4. For this purpose 532 nm laser light is focused by a 20X objective just above a glass sample containing supersaturated aqueous KCl solution. The phenomenon leading up to the crystal formation is then observed visually with the help of a CMOS camera.

3.1. Materials

KCl obtained from Sigma Aldrich with molecular biology > 99.0% is mixed with distilled water from an in-house dispenser (Elga Purelab Ultra, 3.7 MΩ.cm) in order to get aqueous KCl solution of required supersaturation.

3.2. Sample preparation

A small stock solution of KCl is prepared by mixing 40 ml of distilled water with 14.46g of KCl which corresponds to a supersaturation of 1.03 at 23 $^{\circ}C$. The solution is heated and stirred for about two hours at 50 $^{\circ}C$ before being transferred into vials similar to the ones used in the previous experiment. These vials are kept in the oven overnight at 65 $^{\circ}C$ to ensure dissolution of KCl. No chemical has been added to absorb the laser energy to increase the probability of cavitation. A sufficiently high supersaturation which did not lead to a significant number of samples nucleating spontaneously was selected.
To prepare the slides for creating cavitation bubble the following steps were followed:

- Parafilm is cut into proper dimensions to fix the distance between the slides. The thickness of the parafilm is between 0.13 mm-0.17 mm. If the distance between slides needs to be increased, then several layers of parafilm can be stacked on top of each other. Thickness is an important parameter as it decides the amount of allowable volume to work with and varies the volume to surface ratio. A thickness of 0.45 mm of parafilm is used as it is the minimum thickness providing least number of spontaneous nucleation. The dimensions of the glass slide are shown in figure 3.1 where the thickness given ranges from the top surface of upper glass slide to the bottom surface of lower glass slide.
- The parafilm is put on top of a glass slide, with dimensions 24x50 mm, on all four sides. As the parafilm can overlap at the edges, the distance between the slides can increase.
- The solution is then taken out of the oven and a controlled volume of solution is put on the centre of the glass slide using a micropipette. For the thickness mentioned previously upto 15 microlitre can be used, without the solution touching the parafilm on the side.
- To close off, a glass slide of dimension 24x40 mm is used. For sticking the glass slides on the parafilm and to seal any possible gaps, an adhesive (NOA81 Norland optical adhesive) is employed. The glue is then cured under ultraviolet light for 1-2 minutes. Figure 3.2 shows the finished sample.

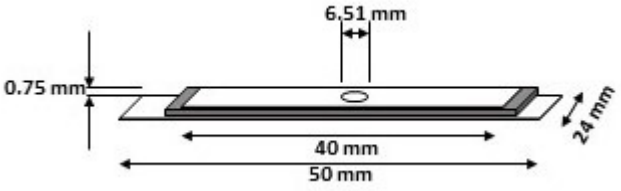

Figure 3.1: Slide dimensions

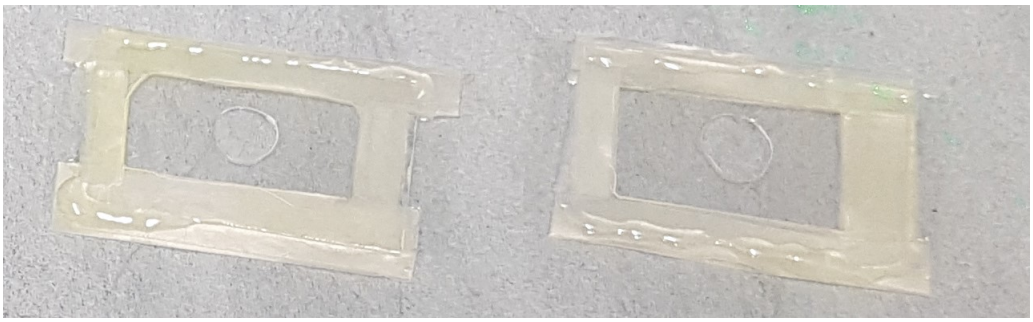

Figure 3.2: Sample after UV curing

- To ensure complete dissolution of samples, the slides are placed back into oven for 10-15 minutes at 45°C. This time was found to be optimum because when kept for long the KCl solution begins to evaporate.

3.3. Experimental setup

The entire setup can be seen in figure 3.3 and has been inspired from a contact lithography station by Patrick Doyle. A visual representation of the setup has also been shown in the figure 3.4. The components of the system are as follows:

3.3.1. Laser source

The same laser source which was used before (section 2.1.3) is now operated at 532 nm by utilizing the second harmonic generation (SHG) process of the potassium dihydrogen phosphate non-linear crystal. As the laser beam is focussed, the power of the beam needs to be reduced drastically. This can be done by changing the orientation of the SHG crystal to the incident laser light or by increasing the Q-Switch delay time. Both of these methods are employed to reduce the power of the laser beam to around 80 mW while maintaining a good beam quality and a stable pulse duration. Moreover, when decreasing the power with help of harmonic generator, there is a minimum that is observed (around 120 mW), beyond which Q-delay needs to be increased. 532 nm was selected for cavitation experiments in order to compare with the existing literature [19]. The duration of laser pulse which is defined as full width at half maximum is about 8.6 ns and measured with the help of a fast photodiode (Thorlabs DET-10).

3.3.2. Mirrors and Iris

Two mirrors (Thorlabs NB1-K13) for the given wavelength are utilised to steer the laser beam into the setup.
An iris is used to select the central part of the beam and reduce the light scattering which can damage some of the components of the setup like the flashlamp and camera.

3.3.3. Beam splitter

A beam splitter (Thor labs CCM1-BS013, 400-700nm) is used to reflect half of the laser beam towards the objective and allows the other half to pass through. The energy of the pulse that enters the objective is monitored thus taking into account the losses through the optical equipment. The beam splitter also allows the white light from the flash lamp to pass through and illuminate the camera

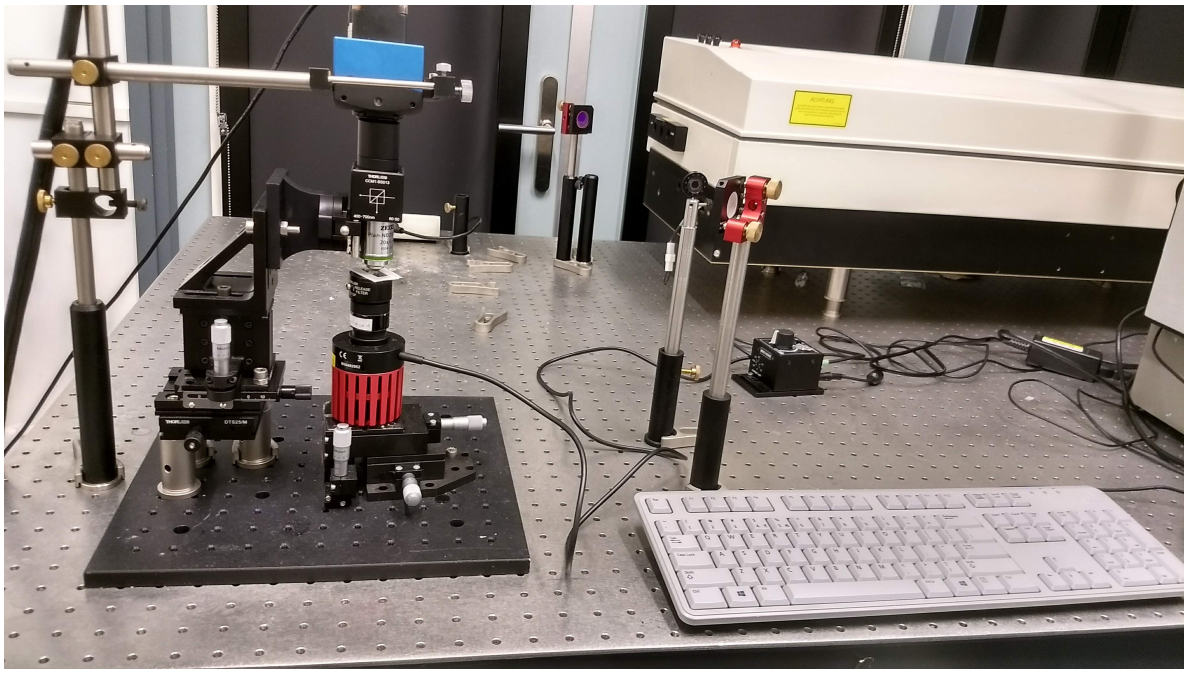

Figure 3.3: The experimental setup to observe cavitation in KCl

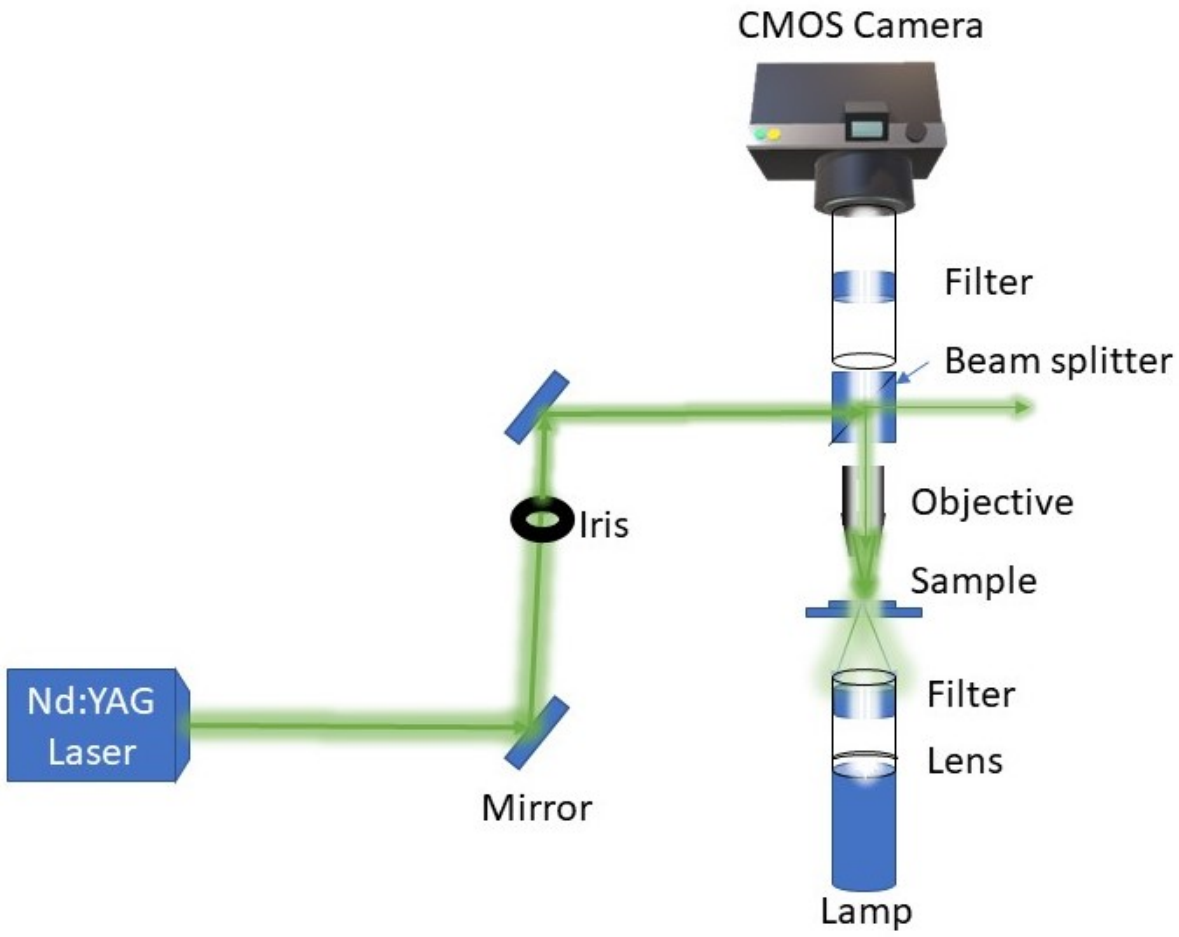

Figure 3.4: Components of the setup

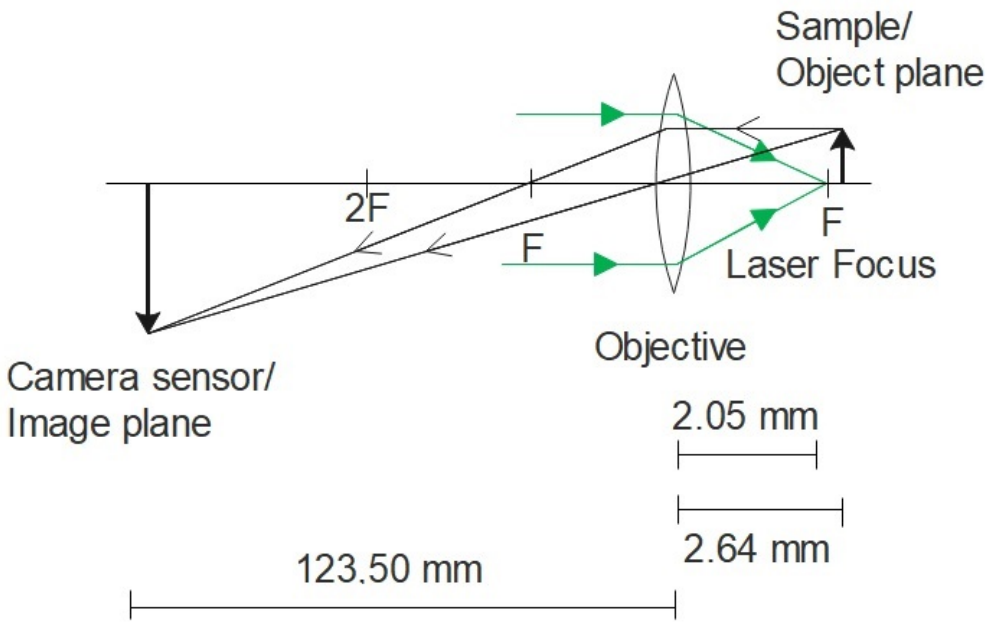

Figure 3.5: Ray diagram for objective lens

sufficiently.

3.3.4. Objective Lens

An objective lens is formed of a system of lenses required to collect light from the object being observed and focus it onto the image plane. Objectives of three different magnifications (4x, 10x, 20x) were tried for our experimental setup. An objective of 20x magnification (Zeiss Plan-Neofluar, NA=0,5) with working distance of 2.05 mm was selected to obtain a tighter focus and to study the process in greater detail. At this magnification the field of view was sufficient to observe the maximum size of the cavitation bubble as reported in literature [19]. The objective focuses the laser near the glass slide so as to induce cavitation in the solution. The focus is kept above the upper glass slide and not in the solution to prevent damages to the slides. This is also done so that the object is after the focus and an image of the solution can be easily formed on the chip of the camera. This has been depicted in figure 3.5. The focal length is measured using micrometer moving stages.

3.3.5. Moving stages

To get the correct alignment for all the components both vertically and horizontally, the setup was designed so that the lamp and objective can be aligned with the help of 2 independent sets of 3 translation stages that move in each directions with an accuracy of 5 microns. The slide is placed on top of the white lamp which can be tweaked for correct alignment. This is done to not move the objective too much as it can lead to part of the beam being blocked by the beam splitter case and to avoid moving the camera every-time with the objective.

3.3.6. Flashlamp

A high intensity white light flashlamp with lens is used for proper illumination of the object. High intensities are required for high speed cameras (short shutter time) and for objectives with higher magnifications. The flash lamp has to be powerful enough to provide sufficient illumination to the sample and the camera, even at low shutter speeds (high frame rate). Figure 3.6 shows the image of KCl crystal taken at a shutter speed of 100 μs (10000 fps).

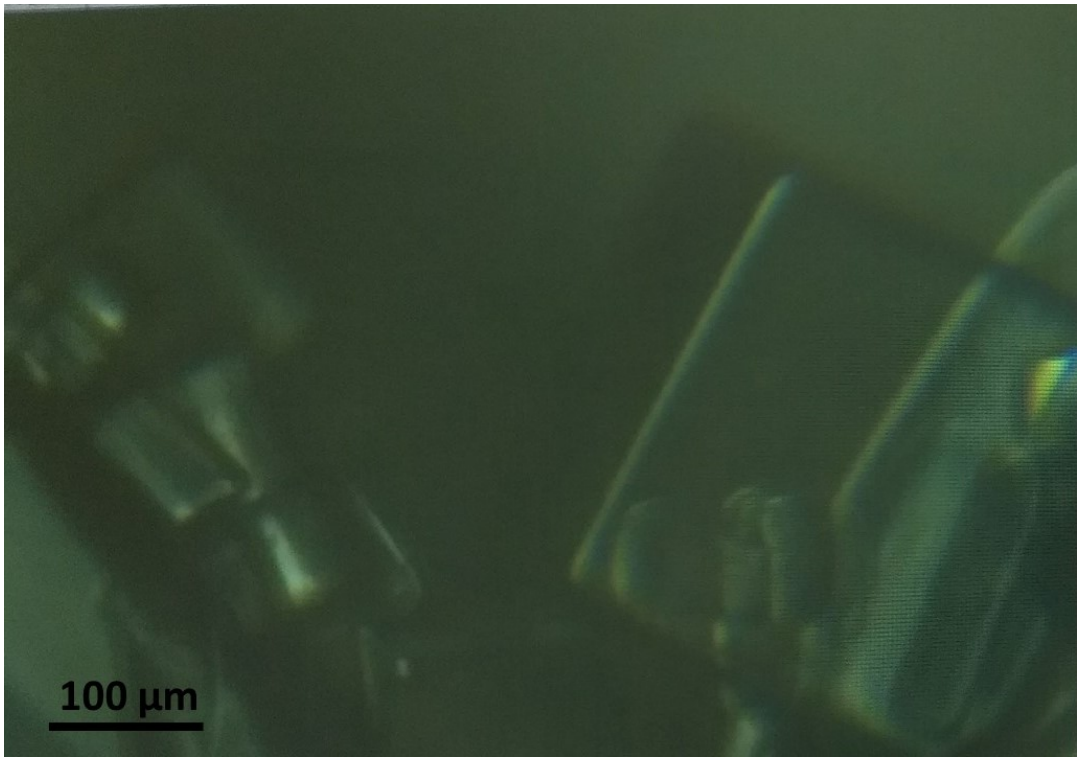

Figure 3.6: Image of KCl crystals at a shutter speed of 100 μs

3.3.7. Filter

As the photons of the laser light are highly coherent, even a small amount of stray light can easily damage the elements of the white lamp or of the detection camera. A bandblock filter centered at 533 nm was selected to prevent damages.

3.3.8. Camera

For safety reasons, the sample was initially imaged with a low-cost camera from Eakins. This camera could only show the image and not record it. After completing safety checks, a high frame rate camera (EO Sens 3CL MC3010) allowed for better specifications including resolution, field view and recording capabilities. The stand of the camera was prepared separately, so as to be able to secure it and move it independently from the setup. The type and capabilities of the camera have been given in section 3.4. As the camera can be easily damaged by the coherent laser photons, it was placed at the top of the setup instead of lying collinearly to the laser beam. The camera still needs to be protected from the reflected as well as scattered laser light, and the lamp also from the direct laser light. For this purpose, the correct filters need to be used and the setup should be covered as much as possible. The power of the reflected laser light reaching the camera ranges from 200 to 300 mW and is measured on various occasions. To reduce this power a variety of filters including notch filters, long pass filters, ND filters and coated KG3 filters were tested. The NF533-17 notch filter and long pass filter were able to provide sufficient protection and reduce the power below the order of μW. In the end, two notch filters seemed to be the best choice at the expense of the long pass filter which removes a major portion of the white light spectrum of the flash lamp.

3.4. Capabilities of the setup

The imaging capabilities of the setup designed and tested will be discussed in this section.

3.4.1. Spatial resolution

The microtron camera (EO Sens 3CL MC3010) consists of a CMOS chip with an active area of 13,57x13,68 mm^2. This chip is divided into 1696x1710 square pixels of size 8 microns. As an objective 20x magnification is used, a more detailed image is obtained but the observation area is reduced. The effective object area which is imaged as well as the pixel size of the image is calculated with the help of the moving stages and the imaging software Streampix 5 by the following method.

- A sample consisting of KCl crystals is imaged and a sharp end of the crystal is brought to the edge of the screen. The corresponding reading of the micrometer is noted.
- The end of the crystal is then brought to the other edge of the screen and the micrometer reading is noted again. This procedure is done once in both horizontal and vertical directions.
- As the resolution of the image is known, the difference between the micrometer readings is divided by the number of pixels of the image.
- This procedure was repeated for three different image resolutions (960x720,1680x1710,640x480) to be precise with the measurements. Every time the image pixel size obtained was 0.729 μm in both horizontal and vertical directions.

3.4.2. Temporal resolution

To be able to conclusively prove the presence of cavitation as a mechanism for NPLIN a very high temporal resolution is required. The time between each frame should be in the order of microseconds, as has been previously reported in literature [18, 19]. Although the camera in use has the capability to reach such high frame rates (180,000) with reduced resolution, the highest frame rate achieved is 330 fps corresponding to approximately 3 ms of time between consecutive images. This is due to the restrictions caused by the buffer storage, image quality and the software.

3.5. Observations

Before detecting cavitation, the crystallization is induced at different laser powers to find the ideal conditions for the observation of the cavitation bubble. Even at the same power the number of pulses required to achieve crystallization varies from 1 to a few (>5). This was obtained from visual observation of 20 slides that were exposed for this purpose to 80-120 mW. Crystals always appear within a few seconds after the firing of a laser pulse.
With the limited capabilities of the camera with respect to the temporal resolution, the cavitation bubbles could not be detected, but a few other observations were made which points towards their presence.

- As can be seen in figure 3.7(a) and (b), because of the laser shot some of the particles are displaced from their position. These could have been carried away due to bubble expansion.
- The crystals were forming at a certain distance from the spot of the laser, this distance was in the same order as the size of the cavitation bubble reported [18, 19]. Also the timeline followed for the development of the crystal is quite similar.
- The crystals start forming around a center as shown in figure 3.7(c). Furthermore, crystals are obtained at multiple locations which points towards the possibility of the bubble surface being an active agent either via accumulation or acting as a site for heterogeneous nucleation.

The above observations points toward the possibility of formation of cavitation bubbles which can play a role in formation of KCl crystals via NPLIN. The following should be taken care of when using software Streampix 5.

- When using an image resolution less than the size of the chip, the region of interest (ROI) begins from the upper left corner of the chip.
- The number of pixels for the region of interest should be higher than the image resolution to avoid any bifurcation of the image.
- To avoid the frame rate being dropped during recording, the frame rate mentioned in Streampix 5 should be less than the one mentioned in MC Control tool (software for the camera).

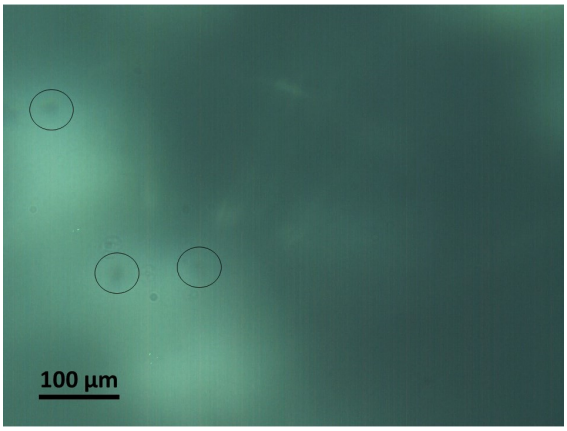

(a) Before the laser shot

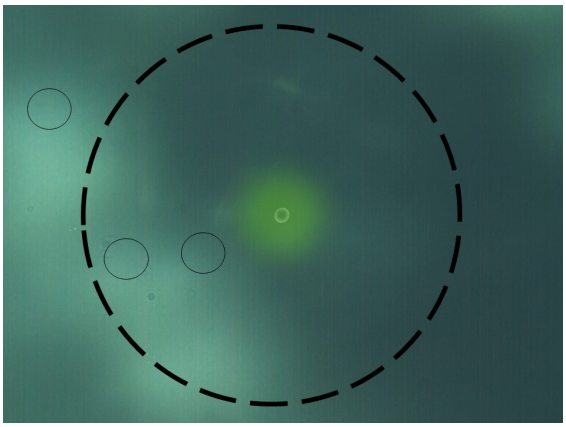

(b) 8 ms after the laser shot. The laser focus is represented by the green spot. The expected size of the cavitation bubble has been shown by the dotted black circle.

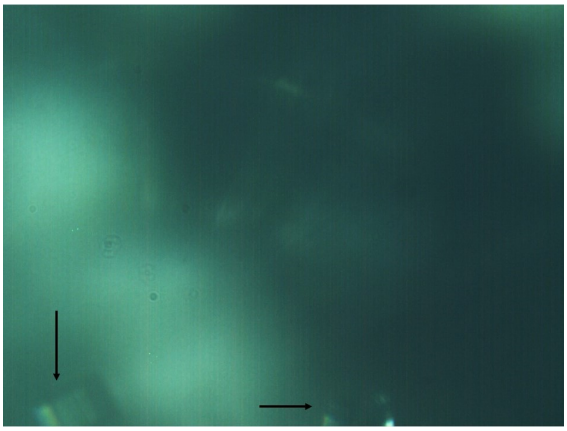

(c) After 60 seconds

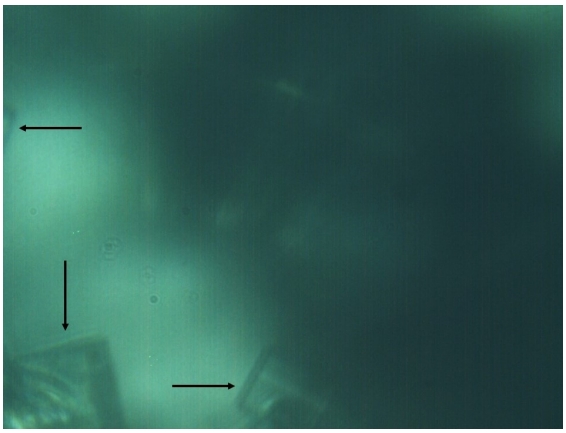

(d) After 120 seconds

Figure 3.7: The formation of crystals with time as observed using the setup. The laser is shot at the center of the frame. The dimensions of the frame are 700x525 μm^2

4

Discussion, Conclusions and Recommendations

4.1. Discussion

This section looks into the implications of the results obtained in the previous two chapters for the mechanism that is followed by NPLIN.

4.1.1. Optical kerr effect

Since the discovery of NPLIN, the optical kerr effect (OKE) has been thoroughly researched as the possible mechanism. The main observation which supports the OKE mechanism is the polarization switching effect proposed by Sun et al [1, 3, 29]. The polarization switching window for glycine stretches between supersaturation of 1.45 and 1.55. At supersaturation below 1.45, only alpha polymorph crystallizes regardless of the polarization state of light . Within the window, linearly polarized light delivers gamma polymorph and circularly polarized light forms alpha polymorph. Beyond the window only gamma polymorph is obtained irrespective of polarization conditions. All the research related to the polarization switching of glycine has been summarized in Table 4.1.
The results shown in chapter 2 can be used to conclude that polarization switching doesn't exist for glycine. This is mainly because of the following reasons:

- There is no difference in the polymorph formation observed for linear and circular polarized light. This is found to be true irrespective of the number of pulses.
- There is definitely an increase in the percentage of gamma polymorph with supersaturation. Hence the increase in gamma polymorph obtained before and after the window is not only a contribution of the laser, but also of the supersaturation.

The absence of this window has also been reported by Liu et al [24]. Clair et al [25] and Javid et al [17], though do not specifically state the absence of such a window, they also contest the results reported by Sun [1].
There are two main reasons why the result obtained by Sun et al [1] is invalid.

- Sun et al expose the vials to 600 pulses at 1064 nm and at power density similar to ours. As has been observed in section 2.2.1 that exposure to a large number of pulses leads to significant reduction in supersaturation. Moreover, such change in supersaturation spans beyond the window itself.
- Although Sun et al used 1200 vials, they ended up with only 10 vials for each data point due to the high number of variables. Their approach resulted in large uncertainities in the values obtained. For a nucleation probability of 0.5, a low number of samples can correspond to approximately 32% error on either side for 95% confidence interval. Due to the stochastic nature of crystallization, a value anywhere between 0.18 and 0.82 is obtained instead of 0.5, the value to which an infinite number of experiments would converge.

Table 4.1: Research till now on polymorphism of glycine via NPLIN

Research paper	Glycine used	Number of pulses	Power Density	Cooling	Aging	Samples per reading	Polarisation switching support
Myerson 2001	S=1,38-1,45	Exposure of several minutes to 10 Hz frequency	0,7 GW/cm^2 at 1064 nm, LP.	50-21°C	Aged at 50°C for several days. For 4 days at 21°C	-	The vials exposed to laser showed majorly γ polymorph with small percentage of α. Control samples only showed α polymorph.
Myerson 2002	S=1,38-1,45	600	0,7GW/cm^2 at 1064nm	69-21°C overnight	Aged for 3-8 days at 21°C	18 exposed to CP light and 46 for LP.	CP light gave α polymorph and LP light gave γ polymorph.
Sun 2006	Glycine>99,7%, S=1,19-2,00	600	0,46GW/cm^2 at 1064, 0,24GW/cm^2 at 532	69°C-room temperature overnight	At 69°C for 2-3 days. Aged for 1-4 days.	60 for each concentration, divided among 6 temperatures.	At all concentrations spontaneous nucleation gave α polymorph. Polarisation switching window concept introduced. Window is narrower for lower intensities and is different for 1064 nm and 532 nm.
Javid 2014	Glycine (Sigma -Aldrich, electrophoresis ≥99%) S=1,4-1,6	600	0.47GW/cm^2 at 1064 nm	cooled for 3-4 hours from 60-25°C	Maintained at 25°C for 20 hours.	Peltier temperature controlled sample holder. Atleast 50 samples used per supersaturation. Used only LP light	Spontaneous nucleation always gave α polymorph. Majority α polymorph is obtained at 1,4 which reduces on increasing the supersaturation. Contests results by Sun.
Bertrand Clair 2014	γ glycine. S=1,0-2,0	600	0.68GW/cm^2 at 532 nm. Laser exposed from top to avoid focussing.	Cooled from 60-17°C in 3 hours and 35 minutes.	Maintained at 17°C for 12 hours.	Temperature controlled sample holder. 10 samples used for each supersaturation. For polymorph characterization no more than 7 vials had crystallized.	Spontaneous nucleation always gave α polymorph. For CP above S=1,56, mostly γ polymorph was obtained and below which α. For LP only α polymorph was obtained. The effect of polarisation is not as strong as that reported by Sun.
Alexander 2017	α+γ glycine Sigma Aldrich (33226, purissp. a., 99.7–101%). S=1,4-1,7	600	0.5GW/cm^2 at 1064 nm.	-	Dissolved at 60-70°C for 2-4 days. Kept for 4 days at 25°C.	Vials not filled till the top. 98 for S=1,4, 91 for S=1,5, 32 for S=1,6 and 12 for S=1,7	Spontaneous nucleation gave mostly α polymorph. Disagrees with Sun's polarisation window. On increasing supersaturation the polymorph changes from α to γ. This transition occurs between 1,4 and 1,5.

Although polarization switching has not been observed, there is a significant effect of laser on the polymorphism because majorly alpha glycine is obtained under S=1.4 and almost completely gamma glycine is obtained at a supersaturation above 1.5. So, the effect of electric field on NPLIN cannot be entirely dismissed.

4.1.2. Cavitation

As the role of electric field in inducing nucleation is not prominent, the focus moves towards the cavitation mechanism. This is supplemented by the fact that absorption of laser light is observed to cause changes in temperature of the solution. This makes the absorption by impurities much more probable. The observation made with the help of the experimental setup designed in chapter 3 points towards the role of cavitation mechanism for crystallization of KCl. The presence of a bubble is suspected due to formation of crystals at multiple points around the laser focus and at a distance quite similar to the diameter reported before.
The previous cavitation experiments [18, 19], are distinct from other NPLIN studies [12]. To bridge the gap, the new setup features the following modifications: the laser light is focused above the sample; the solution is highly transparent to light wavelength.

4.2. Conclusions

- The use of laser drastically reduces the induction time for glycine crystallization.
- There is a polymorph dependence of glycine on supersaturation. This effect is exacerbated by the use of laser as it increases the tendency of formation of alpha polymorph at lower supersaturation (S=1.4) and gamma polymorph at higher supersaturation(S≥1.5).
- No difference in nucleation and polymorph formation is found by changing the polarization of light, thus polarization switching window is not observed.
- Exposure to 600 pulses results in a significant decrease of supersaturation. Any observations made for NPLIN research of glycine at this number of pulses is shadowed by the uncertainty in the real value of the reported supersaturation.
- The cavitation setup designed can produce images with pixel size as small as 0.729 μm and can reach a frame rate up to 330 fps.
- The absence of polarization switching effect in conjunction with temperature increase due to absorption of laser light, improve the chances of cavitation being the governing mechanism behind nucleation. This is supplemented by the observations made in chapter 3, which definitely point towards the presence of a bubble.

4.3. Recommendations

This report has tried to further the understanding of NPLIN mechanism, but there still is a long way to go. The future steps I would recommend to be taken of are as follows:

- To further test the role of cavitation, the following experiments can be conducted.
  - Observe the difference in cavitation and crystallization by using the setup designed in chapter 3 for filtered and unfiltered KCl.
  - Study the effect of laser power in more detail. As the power utilized in this report was sufficient to induce crystallization, so the effect can be tested at lower powers.
  - Observe the cavitation effect in distilled water and compare it with the results obtained for KCl.
- One of the major issues with any crystallization experiment is the stochasticity of the process. As the laser can be focused into small volumes, the use of the cavitation setup in combination with a microfluidic chip will greatly help in achieving trends with high accuracy.

- The polarization switching window was not observed for glycine, but to rule out Optical Kerr effect, other chemicals also need to be studied. Chemicals like Urea and L-Histidine can be used for this purpose as they have been reported to exhibit polarization switching effect.
- A more detailed comparison should be done between the polymorph formation by crash cooling and laser exposure with respect to time at the remaining supersaturations.

A

Tabulated results for glycine research

This section gives in detail all the results that were obtained for the study of NPLIN in glycine.

A.1. S=1.4

A.1.1. 600 pulses

Linear polarisation, 600 pulses, 1064 nm, Batch 8					
Amount exposed	Hours after exposure	Amount nucleated (Cumulative)	Cumulative %	Polymorph with quantity	% gamma polymorph
77	7	1	1.3	1 Alpha	0
	24	5(6)	7.8	5 Alpha	0
	48	3(9)	11.7	3 Alpha	0

Circular polarisation, 600 pulses, 1064 nm, Batch 8					
Amount exposed	Hours after exposure	Amount nucleated (Cumulative)	Cumulative %	Polymorph with quantity	% gamma polymorph
79	7	2	2.5	2 Alpha	0
	24	2(4)	5.1	2 Alpha	0
	48	1(5)	6.3	1 Alpha	0

With the remaining 142 samples the experiment was repeated, but this time no nucleation was obtained.

A.1.2. 1 and 100 pulses

Linear polarisation, 1 pulse, 532 nm				
Amount exposed	Hours after exposure	Amount nucleated	Cumulative %	% gamma polymorph
35	7	0	0	0
	24	0	0	0
	48	0	0	0

Linear polarisation, 100 pulses, 532 nm					
Amount exposed	Hours after exposure	Amount nucleated	Cumulative %	Polymorph with quantity	% gamma polymorph
35	7	3	8.5	2 Alpha and 1 gamma	33.33
	24	0	8.5	0	0
	48	0	8.5	0	0

Linear polarisation, 100 pulses, 532 nm					
Amount exposed	Hours after exposure	Amount nucleated	Cumulative %	Polymorph with quantity	% gamma polymorph
30	7	1	3.33	1 Alpha	0
	24	0	0	0	0
	48	0	0	0	0

A.1.3. Crash cooling

Crash cooled					
Amount crash cooled	Hours after crash cooling	Amount nucleated (Cumulative)	Cumulative %	Polymorph	%gamma polymorph
71	7	0 (0)	0	0	0
	24	6 (6)	8.45	6 alpha	0
	48	6 (12)	16.90	5 alpha & 1 alpha+gamma	0
	72	21(33)	46.47	19 alpha & 2 gamma	9.52
	120	8(41)	57.74	7 alpha & 1 gamma	12.5

The overall percentage of gamma polymorph obtained was 7.3.

A.2. S=1.5

A.2.1. 1 pulse

Linear polarisation, 1 pulse, 1064 nm, 1st round, Batch 6					
Amount exposed	Hours after exposure	Amount nucleated (Cumulative)	Cumulative %	Polymorph	%gamma polymorph
63	7	23 (23)	36.5	4 alpha & 19 gamma	82.6
	24	5 (28)	44.4	1 alpha & 4 gamma	80
	48	5 (33)	52.4	2 alpha & 3 gamma	60

Circular polarisation, 1 pulse, 1064 nm, 1st round, Batch 6					
Amount exposed	Hours after exposure	Amount nucleated (Cumulative)	Cumulative %	Polymorph	%gamma polymorph
63	7	17 (17)	27	1 alpha & 16 gamma	94.1
	24	4 (21)	33.3	2 alpha & 2 gamma	50
	48	5 (26)	41	4 alpha & 1 gamma	20

Linear polarisation, 1 pulse, 1064 nm, 2nd round, Batch 6					
Amount exposed	Hours after exposure	Amount nucleated (Cumulative)	Cumulative %	Polymorph	%gamma polymorph
57	7	9 (9)	15.8	9 gamma	100
	24	2 (11)	19.3	1 alpha & 1 gamma	50
	48	0 (11)	0	0	0

Circular polarisation, 1 pulse, 1064 nm, 2nd round, Batch 6					
Amount exposed	Hours after exposure	Amount nucleated (Cumulative)	Cumulative %	Polymorph	%gamma polymorph
45	7	4 (4)	8.88	3 gamma & 1 alpha+gamma	75
	24	2 (6)	13.3	1 alpha & 1 alpha+gamma	0
	48	0 (6)	0	0	0

Linear polarisation, 1 pulse, 1064 nm, 3rd round, Batch 9					
Amount exposed	Hours after exposure	Amount nucleated (Cumulative)	Cumulative %	Polymorph	%gamma polymorph
68	7	10 (10)	14.7	1 alpha & 9 gamma	90
	24	0 (10)	14.7	0	0
	48	2 (12)	17.6	2 gamma	100
	72	2(14)	20.6	1 alpha & 1 gamma	50

Circular polarisation, 1 pulse, 1064 nm, 3rd round, Batch 9					
Amount exposed	Hours after exposure	Amount nucleated (Cumulative)	Cumulative %	Polymorph	%gamma polymorph
68	7	13 (13)	19.1	3 alpha & 10 gamma	77
	24	1 (14)	20.6	1 gamma	100
	48	1 (15)	22.1	1 gamma	100
	72	1(16)	23.5	1 alpha	0

Linear polarisation, 1 pulse, 1064 nm, 4th round, Batch 9					
Amount exposed	Hours after exposure	Amount nucleated (Cumulative)	Cumulative %	Polymorph	%gamma polymorph
50	7	4 (4)	8	1 alpha and 3gamma	75
	24	2 (6)	12	2 gamma	100

Linear polarisation, 1 pulse, 1064 nm, 5th round, Batch 11			
Amount exposed	Hours after exposure	Amount nucleated (Cumulative)	Cumulative %
70	7	11 (11)	16
	24	4 (15)	21

Linear polarisation, 1 pulse, 1064 nm, 6th round, Batch 11			
Amount exposed	Hours after exposure	Amount nucleated (Cumulative)	Cumulative %
70	7	9 (9)	13
	24	1(10)	14

A.2.2. 600 pulses

Linear polarisation, 600 pulses, 1064 nm, 1st round, Batch 7					
Amount exposed	Hours after exposure	Amount nucleated (Cumulative)	Cumulative %	Polymorph	%gamma polymorph
81	7	9 (9)	11.1	4 gamma & 5 alpha	44
	24	0(9)	0	0	0
	48	4 (13)	16	4 alpha	0

Circular polarisation, 600 pulses, 1064 nm, 1st round, Batch 7					
Amount exposed	Hours after exposure	Amount nucleated (Cumulative)	Cumulative %	Polymorph	%gamma polymorph
81	7	6 (6)	7.4	4 gamma & 2 alpha	67
	24	0	0	0	0
	48	1 (7)	8.64	1 alpha	0

Linear polarisation, 600 pulses, 1064 nm, 2nd round, Batch 9					
Amount exposed	Hours after exposure	Amount nucleated (Cumulative)	Cumulative %	Polymorph	%gamma polymorph
50	7	12 (12)	24	1 alpha and 11 gamma	92
	24	0 (12)	24	0	0

A.2.3. Crash cooling

Crash cooled					
Amount crash cooled	Hours after crash cooling	Amount nucleated (Cumulative)	Cumulative %	Polymorph	%gamma polymorph
81	7	0 (0)	0	0	0
	24	3 (3)	3.7	2 alpha & 1 gamma	33
	48	15 (18)	22.22	12 alpha & 3 gamma	20
	96	2 (20)	24.69	3 alpha & 1 gamma	25
	120	6(26)	32.09	3 alpha & 1 gamma	25

The percentage of gamma polymorph obtained was 23.1.

A.3. S=1.6

A.3.1. 1 pulse

Linear polarisation, 1 pulse, 1064 nm, 1st round Batch 10					
Amount exposed	Hours after exposure	Amount nucleated (Cumulative)	Cumulative %	Polymorph	%gamma polymorph
70	7	8 (8)	11.4	1 alpha & 7 gamma	87.5
	24	0 (8)	11.4	0	0
	48	1 (9)	12.9	1 gamma	100
	72	1(10)	14.3	1 alpha	0

Circular polarisation, 1 pulse, 1064 nm, 1st round Batch 10					
Amount exposed	Hours after exposure	Amount nucleated (Cumulative)	Cumulative %	Polymorph	%gamma polymorph
70	7	9 (9)	12.9	9 gamma	100
	24	1 (10)	14.3	1 gamma	100
	48	3 (13)	18.6	2 alpha & 1 alpha+gamma	0
	72	6(19)	27.1	4 alpha & 2 gamma	33

Linear polarisation, 1 pulse, 1064 nm, 2nd round Batch 11			
Amount exposed	Hours after exposure	Amount nucleated (Cumulative)	Cumulative %
71	7	43 (43)	61
	24	6 (49)	69

Linear polarisation, 1 pulse, 1064 nm, 3rd round Batch 11			
Amount exposed	Hours after exposure	Amount nucleated (Cumulative)	Cumulative %
70	7	48 (48)	68
	24	1 (49)	70

A.3.2. 600 pulses

Linear polarisation, 600 pulses, 1064 nm, 1st round Batch 10					
Amount exposed	Hours after exposure	Amount nucleated (Cumulative)	Cumulative %	Polymorph	%gamma polymorph
51	7	14 (14)	27.5	14 gamma	100
	24	0 (14)	27.5	0	0
	48	0 (14)	27.5	0	0
	72	0 (14)	27.5	0	0

Circular polarisation, 600 pulse, 1064 nm, 1st round Batch 10					
Amount exposed	Hours after exposure	Amount nucleated (Cumulative)	Cumulative %	Polymorph	%gamma polymorph
51	7	25 (25)	49	25 gamma	100
	24	0 (25)	49	0	0
	48	0 (25)	49	0	0
	72	3 (28)	55	3 alpha	0

A.3.3. Crash cooling

Crash cooled 1st round			
Amount crash cooled	Hours after crash cooling	Amount nucleated (Cumulative)	Cumulative %
65	7	0 (0)	0
	24	9 (9)	13.8
	96	8 (17)	26.2
	120	1 (18)	27.7
	144	9(27)	44

Crash cooled 2nd round			
Amount crash cooled	Hours after crash cooling	Amount nucleated (Cumulative)	Cumulative %
69	7	1 (1)	1.4
	24	18 (19)	27.5
	48	37 (56)	81.2
	96	2 (58)	84.1
	120	0(58)	84.1

The cumulative percentage of gamma polymorph obtained was 51.8.

A.4. S=1.7

A.4.1. 1 pulse

Linear polarisation, 1 pulse, 1064 nm, 1st round Batch 11			
Amount exposed	Hours after exposure	Amount nucleated (Cumulative)	Cumulative %
70	7	49 (49)	69
	24	7 (56)	79
	48	0 (56)	79

Linear polarisation, 1 pulse, 1064 nm, 2nd round Batch 11			
Amount exposed	Hours after exposure	Amount nucleated (Cumulative)	Cumulative %
68	7	59 (59)	87
	24	0 (59)	87
	48	0 (59)	87

A.4.2. Crash cooling

Crash cooled			
Amount exposed	Hours after exposure	Amount nucleated (Cumulative)	Cumulative %
68	7	7 (7)	10
	24	2 (9)	13
	48	39 (46)	67
	96	11(57)	84
	120	1(58)	85

The percentage of gamma polymorph formed was 63.8.

B

Error bar calculation

Crystallization being a stochastic process, is something which cannot be controlled fully. This becomes a major source of error when experiments are performed. So calculation of error bars is important.

B.1. Error in a single experiment

In NPLIN, in a set of n vials being exposed, every vial acts as an individual experiment with the whole set of n vials giving a mean probability of nucleation (μ) with a standard deviation (σ). As the standard deviation represents the variation for the entire population (Infinite samples), so to calculate the error for sample population a different parameter is calculated which is called standard error (SE). The formulas used are as follows:

$$\mu = x/n \tag{B.1}$$

Where,
x= The number of vials that crystallized from the total sample of n vials.
As the population standard deviation is unknown, instead the sample standard deviation (σ_s is used for the calculations

$$\sigma_s = \sqrt{\frac{\sum_{i=1}^{n}(x_i - \mu)^2}{n}} \tag{B.2}$$

Where,
x_i= 0, if the vial didn't show crystallization and 1 if it did.

$$SE = \frac{\sigma_s}{\sqrt{n}} \tag{B.3}$$

The error in value of the number of vials that crystallized with 95% confidence limit is given by multiplying the standard error by 1.96.
As an example, a calculation of the standard error for probability of nucleation in the case of an aqueous glycine solution of S=1.6 and exposed to 600 pulses of circularly polarised light is shown. In this case 25(x) vials crystallized out of 51(n). This gives

μ=0.49
σ_s=0.49
SE=0.070

Standard error with 95% confidence limit is equal to 0.13. So the value for probability of nucleation can lie anywhere between 0.36-0.62.

B.2. Cumulative error in multiple experiments

For most of the experiments, to get a direct comparison for different parameters and to reduce the error in values obtained they were repeated multiple times. As the number of vials used and the amount of nucleation obtained every time is different, the results need to be properly combined with weights(w_i) given to each experiment. The weight is defined as the inverse of the square of standard error.
The cumulative nucleation probability mean (μ_n) is given as [30]:

$$\mu_n = \frac{\sum_{i=1}^{k} \mu_i * n_i}{\sum_{i=1}^{k} n_i} \tag{B.4}$$

Where,
k= Number of different experiments
μ_i= Nucleation probability mean of i^{th} experiment
n_i= Number of vials used in i^{th} experiment
Cumulative standard error (SE_n) is given by [30]

$$SE_n = \sqrt{\frac{1}{{w_i}^2} * \frac{\sum_{i=1}^{k} \mu_i * (1-\mu_i) * {w_i}^2}{\sum_{i=1}^{k} n_i}} \tag{B.5}$$

The final error in the cumulative mean is calculated similar to the previous section from the standard error for a confidence limit of 95%.

Bibliography

[1] X. Sun, B. A. Garetz, and A. S. Myerson, *Supersaturation and polarization dependence of polymorph control in the nonphotochemical laser-induced nucleation (nplin) of aqueous glycine solutions,* Crystal growth & design **6**, 684 (2006).

[2] B. A. Garetz, J. Matic, and A. S. Myerson, *Polarization switching of crystal structure in the nonphotochemical light-induced nucleation of supersaturated aqueous glycine solutions,* Physical review letters **89**, 175501 (2002).

[3] X. Sun, B. A. Garetz, and A. S. Myerson, *Polarization switching of crystal structure in the nonphotochemical laser-induced nucleation of supersaturated aqueous l-histidine,* Crystal Growth and Design **8**, 1720 (2008).

[4] J. Zaccaro, J. Matic, A. S. Myerson, and B. A. Garetz, *Nonphotochemical, laser-induced nucleation of supersaturated aqueous glycine produces unexpected γ-polymorph,* Crystal Growth & Design **1**, 5 (2001).

[5] B. Garetz, J. Aber, N. Goddard, R. Young, and A. Myerson, *Nonphotochemical, polarization-dependent, laser-induced nucleation in supersaturated aqueous urea solutions,* Physical review letters **77**, 3475 (1996).

[6] K. Fang, S. Arnold, and B. A. Garetz, *Nonphotochemical laser-induced nucleation in levitated supersaturated aqueous potassium chloride microdroplets,* Crystal Growth & Design **14**, 2685 (2014).

[7] R. Kacker, S. Dhingra, D. Irimia, M. K. Ghatkesar, A. Stankiewicz, H. J. Kramer, and H. B. Eral, *Multiparameter investigation of laser-induced nucleation of supersaturated aqueous kcl solutions,* Crystal Growth & Design **18**, 312 (2017).

[8] M. R. Ward and A. J. Alexander, *Nonphotochemical laser-induced nucleation of potassium halides: Effects of wavelength and temperature,* Crystal Growth & Design **12**, 4554 (2012).

[9] B. C. Knott, M. F. Doherty, and B. Peters, *A simulation test of the optical kerr mechanism for laser-induced nucleation,* The Journal of chemical physics **134**, 154501 (2011).

[10] M. R. Ward, I. Ballingall, M. L. Costen, K. G. McKendrick, and A. J. Alexander, *Nanosecond pulse width dependence of nonphotochemical laser-induced nucleation of potassium chloride,* Chemical Physics Letters **481**, 25 (2009).

[11] M. R. Ward, A. M. Mackenzie, and A. J. Alexander, *Role of impurity nanoparticles in laser-induced nucleation of ammonium chloride,* Crystal Growth & Design **16**, 6790 (2016).

[12] M. R. Ward, W. J. Jamieson, C. A. Leckey, and A. J. Alexander, *Laser-induced nucleation of carbon dioxide bubbles,* The Journal of chemical physics **142**, 144501 (2015).

[13] A. J. Alexander and P. J. Camp, *Single pulse, single crystal laser-induced nucleation of potassium chloride,* Crystal Growth and Design **9**, 958 (2008).

[14] M. R. Ward, S. McHugh, and A. J. Alexander, *Non-photochemical laser-induced nucleation of supercooled glacial acetic acid,* Physical Chemistry Chemical Physics **14**, 90 (2012).

[15] B. C. Knott, J. L. LaRue, A. M. Wodtke, M. F. Doherty, and B. Peters, *Communication: Bubbles, crystals, and laser-induced nucleation,* (2011).

[16] N. Mirsaleh-Kohan, A. Fischer, B. Graves, M. Bolorizadeh, D. Kondepudi, and R. N. Compton, *Laser shock wave induced crystallization,* Crystal Growth & Design **17**, 576 (2017).

[17] N. Javid, T. Kendall, I. S. Burns, and J. Sefcik, *Filtration suppresses laser-induced nucleation of glycine in aqueous solutions,* Crystal Growth & Design **16**, 4196 (2016).

[18] K. Nakamura, Y. Hosokawa, and H. Masuhara, *Anthracene crystallization induced by single-shot femtosecond laser irradiation: experimental evidence for the important role of bubbles,* Crystal growth & design **7**, 885 (2007).

[19] A. Soare, R. Dijkink, M. R. Pascual, C. Sun, P. W. Cains, D. Lohse, A. I. Stankiewicz, and H. J. Kramer, *Crystal nucleation by laser-induced cavitation,* Crystal growth & design **11**, 2311 (2011).

[20] M. Felix and A. Ellis, *Laser-induced liquid breakdown-a step-by-step account,* Applied physics letters **19**, 484 (1971).

[21] T. Uwada, S. Fujii, T. Sugiyama, A. Usman, A. Miura, H. Masuhara, K. Kanaizuka, and M.-a. Haga, *Glycine crystallization in solution by cw laser-induced microbubble on gold thin film surface,* ACS applied materials & interfaces **4**, 1158 (2012).

[22] H. Y. Yoshikawa, R. Murai, S. Maki, T. Kitatani, S. Sugiyama, G. Sazaki, H. Adachi, T. Inoue, H. Matsumura, K. Takano, *et al.*, *Laser energy dependence on femtosecond laser-induced nucleation of protein,* Applied Physics A **93**, 911 (2008).

[23] T.-H. Liu, T. Uwada, T. Sugiyama, A. Usman, Y. Hosokawa, H. Masuhara, T.-W. Chiang, and C.-J. Chen, *Single femtosecond laser pulse-single crystal formation of glycine at the solution surface,* Journal of Crystal Growth **366**, 101 (2013).

[24] Y. Liu, M. H. van den Berg, and A. J. Alexander, *Supersaturation dependence of glycine polymorphism using laser-induced nucleation, sonocrystallization and nucleation by mechanical shock,* Physical Chemistry Chemical Physics **19**, 19386 (2017).

[25] B. Clair, A. Ikni, W. Li, P. Scouflaire, V. Quemener, and A. Spasojević-de Biré, *A new experimental setup for high-throughput controlled non-photochemical laser-induced nucleation: application to glycine crystallization,* Journal of Applied Crystallography **47**, 1252 (2014).

[26] E. Boldyreva, V. Drebushchak, T. Drebushchak, I. Paukov, Y. A. Kovalevskaya, and E. Shutova, *Polymorphism of glycine, part i,* Journal of thermal analysis and calorimetry **73**, 409 (2003).

[27] B. S. Lark, P. Patyar, T. S. Banipal, and N. Kishore, *Densities, partial molar volumes, and heat capacities of glycine, l-alanine, and l-leucine in aqueous magnesium chloride solutions at different temperatures,* Journal of Chemical & Engineering Data **49**, 553 (2004).

[28] S. Budavari, M. O'Neil, A. Smith, P. Heckelman, and J. Kinneary, *The merck index. an encyclopedia of chemicals, drugs and biologicals. whitehouse station, nj. merck research laboratories division of merck & co,* Inc. Monograph , 4175 (1996).

[29] J. Matic, X. Sun, B. A. Garetz, and A. S. Myerson, *Intensity, wavelength, and polarization dependence of nonphotochemical laser-induced nucleation in supersaturated aqueous urea solutions,* Crystal growth & design **5**, 1565 (2005).

[30] N. M. Laird and F. Mosteller, *Some statistical methods for combining experimental results,* International journal of technology assessment in health care **6**, 5 (1990).